energies

MDPI

Article

Coordinated Planning for Multiarea Wind-Solar-Energy Storage Systems That Considers Multiple Uncertainties

Weijie Wu [1], Yixin Li [1], Shu Wang [2,3,*], Zheng Wang [2], Shucan Zhou [1], Yining Zhang [1] and Minjia Zheng [1]

[1] Guangdong Power Grid Planning Research Center, Guangdong Power Grid Corporation, Guangzhou 510062, China; wuweijie@gd.csg.cn (W.W.); liyixin@gd.csg.cn (Y.L.); zhoushucan@gd.csg.cn (S.Z.); zhangyining@gd.csg.cn (Y.Z.); zhengminjia@gd.csg.cn (M.Z.)
[2] National Key Laboratory of Renewable Energy Grid-Integration, China Electric Power Research Institute, Beijing 100192, China; wangz@epri.sgcc.com.cn
[3] School of Physics, Peking University, Beijing 100871, China
* Correspondence: wangshu2011@pku.edu.cn

Abstract: As the scale of renewable energy sources (RESs) expands, it is essential to optimize the configuration of wind, solar, and storage resources across different areas. Nevertheless, the unavoidable uncertainties associated with both energy supply and demand present significant challenges for planners. This study aims to address the challenge of coordinated planning for multiarea wind-solar-energy storage systems considering multiple uncertainties. First, uncertainties related to future peak demand, thermal generation output boundaries, demand variability, and stochastic unit production are analyzed and modeled on the basis of robust optimization and stochastic programming techniques. Then, a hierarchical coordinated planning model that incorporates both system-wide (SW) and local area (LA) planning models is proposed. The SW planning model is designed to manage the optimal capacity configuration of RESs and energy storage systems (ESSs) within each LA, as well as the operational boundary of LAs. The LA planning models aim to further optimize the capacities of RESs and ESSs and minimize the economic cost within each LA on the basis of local resource characteristics. To achieve the optimal solution, the analytical target cascading (ATC) algorithm is integrated with the column-and-constraint generation (C&CG) algorithm. The simulation results validate the effectiveness and reasonableness of the proposed coordinated planning model, which not only outperforms independent planning approaches but also effectively manages the uncertainties.

Keywords: coordinated planning; renewable energy source; energy storage system; robust optimization; stochastic programming; uncertainty

check for updates

Citation: Wu, W.; Li, Y.; Wang, S.; Wang, Z.; Zhou, S.; Zhang, Y.; Zheng, M. Coordinated Planning for Multiarea Wind-Solar-Energy Storage Systems That Considers Multiple Uncertainties. *Energies* **2024**, *17*, 5242. https://doi.org/10.3390/en17215242

Academic Editor: Branislav Hredzak

Received: 23 August 2024
Revised: 24 September 2024
Accepted: 7 October 2024
Published: 22 October 2024

Copyright: © 2024 by the authors. Licensee MDPI, Basel, Switzerland. This article is an open access article distributed under the terms and conditions of the Creative Commons Attribution (CC BY) license (https://creativecommons.org/licenses/by/4.0/).

1. Introduction

With increasing fossil fuel depletion and environmental pollution, the development of renewable energy sources (RESs), such as wind power and solar photovoltaic (PV) generation, has become vital for countries aiming to achieve a low-carbon economy and a sustainable energy system [1]. However, the inherent randomness, volatility, and unpredictability of renewable energy sources pose considerable challenges for the planning and operation of power systems [2,3]. In this context, power exchange through multiarea coordination has attracted much attention, which leverages the complementary nature of power sources and loads across different areas to balance supply and demand [4,5]. Different areas within a multiarea power system face a range of uncertainties, including fluctuations in RES production and variability of demand, future peak demand, and future output boundaries of thermal plants. Additionally, each area has unique potential for expanding renewable energy sources. Effectively addressing these uncertainties and harnessing area potentials are essential for successful multiarea power system planning and optimization. To improve renewable energy absorption and optimize the performance of interconnected grids, this paper develops a hierarchical coordinated planning model for the capacity

configuration of wind, photovoltaic, and energy storage systems, with a comprehensive consideration of various uncertainties and the complementary characteristics of resources across different areas.

Optimal planning for renewable energy sources has been extensively studied. Social welfare theory was applied to configure the thermal-wind-solar power systems, aiming to achieve a balance between economic efficiency and social benefits [6]. In [7,8], energy storage systems (ESSs) were integrated with the RES to improve the reliability and security. A bilevel planning model was proposed to coordinate distributed generation and energy storage: the upper level determines optimal locations and capacities for these resources whereas the lower level focuses on optimizing the operation of energy storage devices [9]. Additionally, a bilevel carbon-oriented planning approach was developed for energy storage stations in multi-integrated energy systems [10]. The challenge of coordinating renewable generation capacities with energy storage installation for a low-carbon power system was addressed [11]. A nonconvex mixed-integer nonlinear optimization problem, structured as a master–slave model, has been introduced for transmission expansion planning under contingency constraints. This approach integrates various kinds of energy storage systems along with the RES [12]. However, the mentioned studies focused on single-area planning, ignoring the complexities of multiarea planning.

The planning challenge across multiple areas is fundamentally more intricate than that of a single area. Each area may have its own local planner to address their specific challenges independently. This independence can lead to excessive investment costs and diminish the overall efficiency. Many studies assume a central entity with comprehensive grid information that can create a unified planning problem for the entire network. In [13], a detailed expansion method for generation and transmission components in multiarea systems was introduced. In [14], the multiperiod, multiarea generation expansion planning challenge was addressed. In [15], a multiarea capacity expansion model that considers increased renewable energy integration, flexibility constraints, and low-carbon policies was developed. Despite the advantages of a centralized approach in enhancing system performance and reducing costs, this approach often fails to address the unique characteristics and requirements of each area. This lack of area coordination can result in suboptimal outcomes, as it does not fully integrate diverse area aspects into the overall planning process.

The decomposition and coordination method is also effective for addressing multiarea power system planning. In [16], the co-planning of wind farms, energy storage, and transmission lines was solved via partitioning the power system into distinct areas. In [17,18], a two-level distributed optimization algorithm for multiarea power system planning was introduced, where each area acts as a local planner, and a system-wide planner coordinates these local planners. However, the decomposition and coordination method in these studies lacks comprehensive consideration of multiple uncertainty sources, such as renewable energy sources, load demands, and generation operating conditions, leading to the deviations of the optimal planning outcomes from reality.

In research on the RESs and ESSs planning problem, stochastic programming (SP) and robust optimization (RO) are generally applied to model the uncertainties. The uncertainties in the wind and photovoltaic power plant outputs, as well as load uncertainties, are supported by extensive, publicly available historical data. Therefore, SP is suitable for addressing such uncertainties via creating a finite set of scenarios [19]. The k-medoids clustering algorithm has been used to provide a scenario set for the microgrid planning model [20]. Long-term uncertainty in RES output is represented through a scenario tree in the integrated generation, transmission, and energy storage planning model [21]. In the cases where historical data are lacking, RO becomes valuable. This method only requires confidence bounds on uncertainty fluctuations and can ensure that planning results remain robust under extreme conditions. A robust optimization model for the RES and transmission expansion has been suggested [22]. A hybrid RO-SP framework was proposed to enhance unit commitment scheduling [23]. In this approach, SP manages the fluctuations

in solar radiation and RO deals with uncertainties related to pricing. Additionally, a stochastic adaptive robust optimization technique has been created for planning generation and transmission expansion [24]. This technique represents long-term uncertainties using confidence bounds and captures short-term uncertainties through different operational scenarios. By integrating these techniques, the RO-SP framework adeptly manages multiple uncertainty types, providing a robust solution to complex planning challenges.

In practice, simultaneously addressing the challenges of decentralized multiarea and the disturbance features of various uncertainties in the planning process can be particularly complex. This paper addresses the challenge of uncertainties in energy systems through combining stochastic programming and robust optimization techniques to effectively model various uncertainties, including renewable energy sources, future peak load demands, and the boundaries of thermal generation outputs. In addition, a hierarchical coordinated planning model that considers power interconnections between areas is developed. The ATC algorithm is integrated with the C&CG algorithm to identify the optimal capacity configuration of the RES and ESS. This approach is validated through case studies, which reveal that this method not only outperforms independent planning approaches but also effectively manages the uncertainties.

The remainder of this paper is organized as follows: Section 2 outlines the hierarchical framework of the proposed planning model. Section 3 presents the mathematical formulation of the model. Section 4 explains the solution methodology, incorporating the ATC and C&CG algorithms. Section 5 provides simulation results to illustrate the application of the model. Section 6 presents a discussion of the proposed method, analyzing its advantages and potential limitations. Section 7 concludes the paper, summarizing the key findings and implications of this research.

2. Hierarchical Framework of the Coordinated Planning Model

Considering the distinct characteristics and interdependencies between SW planning and LA planning models, this paper proposes a hierarchical coordinated planning approach, as illustrated in Figure 1.

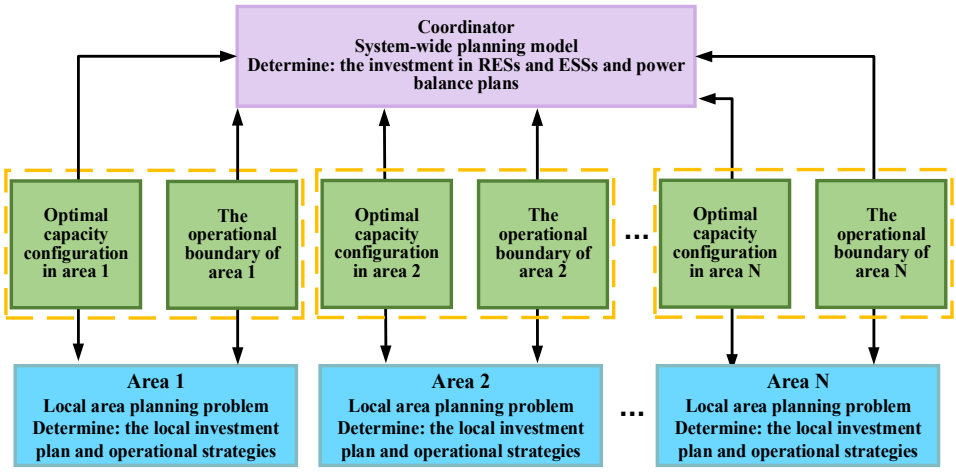


Figure 1. Hierarchical structure of the coordinated planning framework.

The hierarchical framework consists of two layers: the upper-level SW planning model for the whole system and the lower-level LA planning models for each local area. The interaction between these two levels is characterized by a target–response relationship. At the upper level, the SW system planning problem serves as a coordinator, addressing wide-area investment constraints and power balance requirements across the entire region. The SW model develops an initial investment strategy and operational boundary plan on a macro scale for each local area. These initial plans are then transferred to the lower-level LA planning models. Based on local conditions and specific requirements, these LA planning

models refine the initial investment strategy and operational boundary plans. The revised plans from the LA models are then sent back to the upper-level SW model, creating a continuous feedback loop that enhances overall system optimization and responsiveness to local needs. This method not only addresses broad-scale investment concerns but also provides solutions tailored to local conditions, leading to an optimized and cohesive investment plan.

3. Problem Formulation

3.1. Uncertainty Modeling

In this paper, we address multiple uncertainties that influence the formulation of well-informed planning decisions. These uncertainties include future peak demand, the output boundaries of thermal power plants, variability in RES production, and demand fluctuations. This section models these uncertainties according to their specific characteristics.

The outputs of wind and photovoltaic power plants, combined with demand fluctuations, exhibit complex spatiotemporal correlations. To accurately model these uncertainties, we utilize the stochastic programming approach to model them on the basis of historical data. The process for obtaining typical scenarios involves several key steps:

Step 1. Hourly data on load and RES production data are collected for each area. The daily load and RES production values for all the areas are defined as a distinct scenario. This definition ensures that each scenario accurately represents a unique combination of load and production values across different areas and retains the complex spatiotemporal correlation information. Suppose that Z historical scenarios are available.

Step 2. The hourly load is divided by the peak demand to calculate the demand factors for each area.

Step 3. The hourly production is divided by the installed capacity of wind/photovoltaic generation to obtain the RES capacity factors for each area.

Step 4. The K-means clustering technique is applied to group similar data into a set of typical scenarios. A detailed description can be found in [25]. Suppose that S discrete typical scenarios are produced, forming a set of typical scenarios $Q = \{Q_1, Q_2, \cdots, Q_S\}$. Each typical scenario $Q_s (s = 1, 2, \cdots, S)$ includes M_s historical scenarios.

Step 5. The probability distributions of these typical scenarios $P_0 = [p_1^0, p_2^0, \cdots, p_S^0]$ are calculated, where $p_s^0 = M_s/Z (s = 1, 2, \cdots, S)$ represents the probability of the s-th typical scenario.

This approach groups similar historical data, preserving both the variability and correlation information inherent in the data. It is assumed that demand factors and RES capacity factors will remain constant through the planning horizon [26].

Unlike demand factors and RES capacity factors, the future peak demand and the output boundaries of thermal power plants cannot be assumed to be constant. This inherent variability must be carefully considered to ensure accurate and effective planning. Future electricity demand is influenced by socioeconomic factors, which complicates accurate predictions. Similarly, the future output boundaries of thermal power plants are impacted by factors such as unit retirement, malfunctions, maintenance schedules, and start-up plans. Therefore, we utilize robust optimization to model them. The future peak demand and the output boundaries of thermal power plants can be formulated as follows:

$$U^D\left(p_{n,s}^D, \hat{p}_{n,s}^D, \Gamma_{n,s}^D\right) := \left\{ \begin{array}{l} \widetilde{p}_{n,s}^D \in \mathbb{R}^{N\times S} : \sum\limits_{s\in\Omega_s} \dfrac{\left|\widetilde{p}_{n,s}^D - p_{n,s}^D\right|}{\hat{p}_{n,s}^D} \leqslant \Gamma_n^D \\ \widetilde{p}_{n,s}^D \in \left[p_{n,s}^D - \hat{p}_{n,s}^D, p_{n,s}^D + \hat{p}_{n,s}^D\right], \forall n \in \Omega_n, s \in \Omega_s \end{array} \right\}, \tag{1}$$

$$U^{g\max}\left(P_{n,s}^{g\max}, \hat{P}_{n,s}^{g\max}, \Gamma_n^{g\max}\right) := \left\{ \begin{array}{l} \widetilde{P}_{n,s}^{g\max} \in \mathbb{R}^{N\times S} : \sum\limits_{s\in\Omega_s} \dfrac{\left|\widetilde{P}_{n,s}^{g\max} - P_{n,s}^{g\max}\right|}{\hat{P}_{n,s}^{g\max}} \leqslant \Gamma_n^{g\max} \\ \widetilde{P}_{n,s}^{g\max} \in \left[P_{n,s}^{g\max} - \hat{P}_{n,s}^{g\max}, P_{n,s}^{g\max} + \hat{P}_{n,s}^{g\max}\right], \forall n \in \Omega_n, s \in \Omega_s \end{array} \right\}, \tag{2}$$

$$U^{g\min}\left(P_{n,s}^{g\min}, \hat{P}_{n,s}^{g\min}, \Gamma_n^{g\min}\right) := \left\{ \widetilde{P}_{n,s}^{g\min} \in \mathbb{R}^{N\times S} : \sum_{s\in\Omega_s} \frac{\left|\widetilde{P}_{n,s}^{g\min} - P_{n,s}^{g\min}\right|}{\hat{P}_{n,s}^{g\min}} \leqslant \Gamma_n^{g\min} \right. \quad (3)$$
$$\left. \widetilde{P}_{n,s}^{g\min} \in \left[P_{n,s}^{g\min} - \hat{P}_{n,s}^{g\min}, P_{n,s}^{g\min} + \hat{P}_{n,s}^{g\min}\right], \forall n \in \Omega_n, s \in \Omega_s \right\},$$

where n is the index of local areas, and subscript n in the symbols below denotes their values in the n-th area; Ω_n is the set of local areas; s is the index of typical scenarios, and subscript s in the symbols below denotes their values under the s-th typical scenario; Ω_s is the set of scenarios; U^D denotes the robust set of future peak demands; $\widetilde{p}_{n,s}^D$ represents the uncertain peak demand; $p_{n,s}^D$ represents the predicted value of peak demand; $\hat{p}_{n,s}^D$ denotes the deviation from predicted value of peak demand; $\Gamma_{n,s}^D$ denotes the budget of uncertainty of peak demand; $U^{g\min}$ is the robust set of lower output boundaries of thermal plants; $\widetilde{P}_{n,s}^{g\min}$ is the uncertain lower output boundaries of thermal plants; $P_{n,s}^{g\min}$ represents the predicted lower output boundaries of thermal plants; $\hat{P}_{n,s}^{g\min}$ represents the deviation from predicted lower output boundaries of thermal plants; $\Gamma_n^{g\min}$ denotes the budget of uncertainty of the lower output boundaries of thermal plants; $U^{g\max}$ denotes a robust set of peak demands; $P_{n,s}^{g\max}$ is the predicted upper output boundaries of thermal plants; $\hat{P}_{n,s}^{g\max}$ is the deviation from the predicted upper output boundaries of thermal plants; $\Gamma_n^{g\max}$ represents the budget of the uncertainty of upper output boundaries of thermal plants; and $\widetilde{P}_{n,s}^{g\max}$ represents the uncertain upper output boundaries of thermal plants. It is unlikely that all predicted values will face the worst-case scenario simultaneously. Therefore, parameters Γ_n^D, $\Gamma_n^{g\max}$, and $\Gamma_n^{g\min}$ serve to adjust the conservativeness of planning decisions via controlling the number of worst-case scenarios.

3.2. Upper-Level Model for the SW Planning Problem

3.2.1. Objective Function

The upper-level model is designed to strategically configure wind, photovoltaic, and storage capacities across different areas while also developing operational boundary plans for each area. The objective function of this model is designed to minimize the overall costs associated with these configurations and operation strategies. The first term calculates the overall investment cost throughout the entire system. The remaining terms focus on operational costs, which include the penalties cost for curtailing RESs, transmission costs between local areas, and the cost of purchasing electricity from neighboring regions. The objective function of the SW planning problem is formulated as follows:

$$F^{SW} = \min_{\substack{S_{n,r}^{SW}, P_{n,s,t}^{SW} \\ P_n^{cur,SW}, P_{s,t}^{buy}, P_{s,t}^{sell}}} \sum_{n\in\Omega_n}\sum_{r\in\Omega_r} B_{n,r} S_{n,r}^{SW} \frac{\vartheta(1+\vartheta)^{Y^r}}{(1+\vartheta)^{Y^r}-1} + \sigma \sum_{n\in\Omega_n} \lambda^{cur} P_n^{cur,SW} \quad (4)$$
$$+\sigma\left[\sum_{n\in\Omega_n}\sum_{s\in\Omega_s}\sum_{t\in\Omega_T} p_s^0\left(\lambda^{trans} P_{n,s,t}^{SW}\right) + \sum_{s\in\Omega_s}\sum_{t\in\Omega_T} p_s^0 \lambda^{buy} P_{s,t}^{buy}\right]$$

where r represents the index of plants/units; Ω_r represents the set of plants/units, including the wind power plants, solar power plants, and THE ESS; t is the index of time, and subscript t in the symbols below denotes their values at time t; Ω_T is the set of time intervals; $S_{n,r}^{SW}$ represents the installed capacity of asset r determined in the SW planning model; $P_{n,s,t}^{SW}$ is the injected power of local area n to the interconnected grids determined in the SW planning model; $P_n^{cur,SW}$ is the curtailed renewable energy of local area n determined in the SW planning model; $P_{s,t}^{buy}$ is the power fed into the neighboring regions; $B_{n,r}$ is the unit investment cost; Y^r is the service life; ϑ is the discount rate; σ is the equivalence factor between annualized investment cost and operational cost, with a value of 365; λ^{cur} is the penalty cost coefficient of renewable energy curtailment; λ^{trans} is the cost coefficient for

transmission between local areas; p_s^0 is the probability of scenario s; and λ^{buy} is the price of power bought from neighboring areas.

3.2.2. Constraints

(1) Installed capacity constraints of RES and ESS

Considering local natural resources, existing grid infrastructure, and development policies, it is clear that the installed capacities of the RES and ESS in a single area and the total capacities of RESs and ESSs across multiple areas are limited.

$$S_{n,w}^{\min} \le S_{n,w}^{SW} \leqslant S_{n,w}^{\max}, \tag{5}$$

$$S_{n,pv}^{\min} \le S_{n,pv}^{SW} \leqslant S_{n,pv}^{\max}, \tag{6}$$

$$S_{n,ESS}^{\min} \le S_{n,ESS}^{SW} \leqslant S_{n,ESS}^{\max}, \tag{7}$$

$$\Gamma_{w}^{\min} \le \sum_{n\in\Omega_n} S_{n,w}^{SW} \leqslant \Gamma_{w}^{\max}, \tag{8}$$

$$\Gamma_{pv}^{\min} \le \sum_{n\in\Omega_n} S_{n,pv}^{SW} \leqslant \Gamma_{pv}^{\max}, \tag{9}$$

$$\Gamma_{ESS}^{\min} \le \sum_{n\in\Omega_n} S_{n,ESS}^{SW} \leqslant \Gamma_{ESS}^{\max}, \tag{10}$$

where $S_{n,w}^{\min}$, $S_{n,pv}^{\min}$, and $S_{n,ESS}^{\min}$ represent the minimum capacity limits of the wind power plants, photovoltaic power plants, and energy storage systems, respectively; $\Gamma_{w}^{\min}$, $\Gamma_{pv}^{\min}$, and $\Gamma_{ESS}^{\min}$ denote the minimum capacity limits for the total installation of RES plants and ESSs across the entire multiarea system, respectively; $S_{n,w}^{\max}$, $S_{n,pv}^{\max}$, and $S_{n,ESS}^{\max}$ represent the maximum capacity limits of RES plants and ESSs, respectively; $\Gamma_{w}^{\max}$, $\Gamma_{pv}^{\max}$, and $\Gamma_{ESS}^{\max}$ denote the maximum capacity limits for the total installation of RES plants and ESSs across the entire multiarea system, respectively.

(2) Configuration ratio of ESS constraints

Due to government policies, available land areas, and various other factors, the capacity configuration ratio for the ESS relative to the RES is constrained. Equation (11) is implemented to ensure an appropriate configuration ratio between the capacities of ESSs and RESs.

$$\phi_{ESS}^{\min}\left(\sum_{n\in\Omega_n} S_{n,pv}^{SW} + \sum_{n\in\Omega_n} S_{n,w}^{SW}\right) \le \sum_{n\in\Omega_n} S_{n,ESS}^{SW} \leqslant \phi_{ESS}^{\max}\left(\sum_{n\in\Omega_n} S_{n,pv}^{SW} + \sum_{n\in\Omega_n} S_{n,w}^{SW}\right), \tag{11}$$

where $\phi_{ESS}^{\max}$ is the maximum ratio of ESS capacity and $\phi_{ESS}^{\min}$ is the minimum ratio of ESS capacity.

(3) Power flow constraints

Equation (12) addresses the power balance for the entire multiarea system. Equation (13) imposes limits on the amount of power that can be injected from each individual area into the interconnected grid. Equation (14) restricts the power exchanged with external areas. This restriction ensures that interactions with external systems are efficient and balanced.

$$\sum_{n\in\Omega_n} P_{n,s,t}^{SW} + P_{s,t}^{buy} = 0, \tag{12}$$

$$P_{n}^{\min} \le P_{n,s,t}^{SW} \le P_{n}^{\max}, \tag{13}$$

$$P_{\min}^{exter} \le P_{s,t}^{buy} \leqslant P_{\max}^{exter}, \tag{14}$$

where $P_n^{\max}$ is the maximum power injected by area n; $P_n^{\min}$ is the minimum power injected by area n; $P_{\max}^{exter}$ is the maximum power exchanged with the external areas; and $P_{\min}^{exter}$ is the minimum power exchanged with the external areas.

(4) RES curtailment constraints

Equation (15) ensures that the renewable energy curtailment rate across the entire area remains within a practical and acceptable range.

$$\sum_{n\in\Omega_n} P_n^{cur,SW} \leqslant \mu^{cur} \sum_{n\in\Omega_n}\sum_{s\in\Omega_s}\sum_{t\in\Omega_T}\left[\left(S_{n,s}^{w0}+S_{n,w}^{SW}\right)U_{n,s,t}^{w}+\left(S_{n,s}^{pv0}+S_{n,pv}^{SW}\right)U_{n,s,t}^{pv}\right], \tag{15}$$

where $U_{n,s,t}^{w}$ represents the capacity factor of wind power plants; $U_{n,s,t}^{pv}$ represents the capacity factor of photovoltaic power plants; $S_{n,s}^{w0}$ is the capacity of existing wind plants; $S_{n,s}^{pv0}$ is the capacity of existing photovoltaic power plants; μ^{cur} indicates the maximum allowable ratio of renewable energy that can be curtailed.

3.3. Lower-Level Model for the LA Planning Problem

In this paper, each LA planning model is simplified into a single-node problem. This simplification is achieved via consolidating all internal buses within each local area into one node. Within this model, various generation technologies are aggregated and connected to this central node, while load demands are combined to form a unified load representation for the node. This aggregation reduces complexity in the planning process, while still providing a comprehensive view of the local power system.

3.3.1. Objective Function

The objective function of the LA planning model is designed to minimize the expected operational costs, in which generation units and ESSs are scheduled for each typical scenario to resist uncertainties from the future peak demand and the output boundaries of thermal plants. The annualized operational cost in Equation (16) contains the operation cost of thermal plants, the expenses associated with charging and discharging of the ESS, and the penalty cost of RES curtailment. The objective function of the LA planning problem is formulated as follows:

$$F_n^{LA} = \max_{\substack{\widetilde{p}_{n,s}^{D} \\ \widetilde{P}_{n,s}^{g\max},\widetilde{P}_{n,s}^{g\min}}} \min_{\substack{S_{n,r}^{LA},P_{n,s,t}^{LA},P_n^{cur,LA} \\ P_{n,s,t}^{cur,g},P_{n,s,t}^{cur,w},P_{n,s,t}^{pv} \\ P_{n,s,t}^{dis},P_{n,s,t}^{ch},E_{n,s,t}^{ESS},e_{n,s,t}^{ch},e_{n,s,t}^{dis}}} \sigma\sum_{s\in\Omega_s}\sum_{t\in\Omega_T} p_s^0\left[\begin{array}{l} f\left(P_{n,s,t}^{g}\right)+c^{bt}\left(P_{n,s,t}^{dis}+P_{n,s,t}^{ch}\right) \\ +\lambda^{cur}P_{k,s}^{cur,w}+\lambda^{cur}P_{k,s}^{cur,pv} \end{array}\right], \tag{16}$$

where $e_{n,s,t}^{ch}$ indicates the status of the charging power of the ESS; $e_{n,s,t}^{dis}$ indicates the status of the discharging power of ESSs; $f\left(P_{n,s,t}^{g}\right) = a_n\left(P_{n,s,t}^{g}\right)^2 + b_nP_{n,s,t}^{g} + c_n$ represents the operation cost of thermal plants, and a_n, b_n, and c_n are the generator cost coefficients; $P_{n,s,t}^{g}$ is the output power of thermal power plants; $P_{n,s,t}^{dis}$ is the discharging power of the ESS; $P_{n,s,t}^{ch}$ is the charging power of the ESS; $P_{n,s,t}^{cur,w}$ is the curtailed power of wind power plants; $P_{n,s,t}^{cur,pv}$ is the curtailed power of PV plants; $S_{n,r}^{LA}$ is the installed capacity of asset r determined in the LA planning model; $P_{n,s,t}^{LA}$ is the injected power of local area n to the interconnected grids determined in the LA planning model; and $P_n^{cur,LA}$ is the curtailed renewable energy of local area n determined in the LA planning model.

3.3.2. Constraints

(1) Power balance constraints

Equation (17) defines the constraints related to power flow balance, ensuring that the power supply matches the demand and maintains system stability.

$$\begin{aligned}\widetilde{p}_{n,s}^{D}U_{n,s,t}^{load} = \quad & P_{n,s,t}^{g} + (S_{n,w}^{0} + S_{n,w}^{LA})U_{n,s,t}^{w} + \left(S_{n,pv}^{0} + S_{n,pv}^{LA}\right)U_{n,s,t}^{pv} - P_{n,s,t}^{w} - P_{n,s,t}^{pv} \\ & -P_{n,s,t}^{ch} + P_{n,s,t}^{dis} + P_{n,s,t}^{LA}\end{aligned}, \quad (17)$$

where $U_{n,s,t}^{load}$ is demand factor; $P_{n,s,t}^{w}$ is output power of wind power plants; and $P_{n,s,t}^{pv}$ is output power of photovoltaic power plants.

(2) Operation constraints of thermal power plant

Equations (18) and (19) describes the constraints in capacity and the ramp rate of thermal power plants. These equations ensure that generation units operate within their defined limits and adjust at permissible rates.

$$\widetilde{P}_{n,s}^{g\min} \leqslant P_{n,s,t}^{g} \leqslant \widetilde{P}_{n,s}^{g\max}, \quad (18)$$

$$P_{n,s}^{d} \leqslant P_{n,s,t}^{g} - P_{n,s,t-1}^{g} \leqslant P_{n,s}^{\mathrm{u}}, \quad (19)$$

where $P_{n,s}^{\mathrm{u}}$ indicates ramp-up limit of thermal power plants and $P_{n,s}^{d}$ indicates ramp-down limit of thermal power plants.

(3) Operation constraints of ESS

Equation (20) establishes the relationship between the state of charge (SOC) and power for the ESS, while Equation (21) specifies the restrictions on the state of charge. Equation (22) indicates that charging and discharging cannot occur simultaneously. Equation (23) specifies the limits for charging and discharging power. Equations (24) and (25) are introduced using the big-M method, which guarantees that the terms are equal when the corresponding binary variable is set to zero; conversely, when the corresponding binary variable is set to one, the terms remain "open".

$$E_{n,s,t}^{bt} = E_{n,s,t-1}^{bt} + \eta_{n}^{ch}P_{n,s,t}^{ch}\Delta t - \frac{1}{\eta_{n}^{dis}} \times P_{n,s,t}^{dis}\Delta t, \quad (20)$$

$$\mu_{\min}^{ESS}\left(S_{n,ESS}^{0} + S_{n,ESS}^{LA}\right) \leq E_{n,s,t}^{ESS} \leq \mu_{\max}^{ESS}\left(S_{n,ESS}^{0} + S_{n,ESS}^{LA}\right), \quad (21)$$

$$e_{n,s,t}^{dis} + e_{n,s,t}^{ch} \leq 1, \quad (22)$$

$$0 \leq P_{n,s,t}^{dis} + P_{n,s,t}^{ch} \leq \beta_{n}\left(S_{n,ESS}^{0} + S_{n,ESS}^{LA}\right), \quad (23)$$

$$0 \leq P_{n,s,t}^{dis} \leq e_{n,s,t}^{dis}M, \quad (24)$$

$$0 \leq P_{n,s,t}^{ch} \leq e_{n,s,t}^{ch}M, \quad (25)$$

where η_{n}^{ch} is the charging efficiency of ESSs in area n; η_{n}^{dis} is the discharging efficiency of ESSs in area n; $S_{n,ESS}^{0}$ is the capacity of existing ESSs under scenario s in area n; β_{n} is the ratio of energy storage capacity to rated power output; $\mu_{\max}^{ESS}$ is the coefficient corresponding to the maximum SOC; $\mu_{\min}^{ESS}$ is the coefficient corresponding to the minimum SOC; and M is sufficiently large constant.

(4) Operation constraints of RES

Equations (26) and (27) set output power restrictions for wind and photovoltaic power stations. The actual output of the RES is limited due to the installation capacity and capacity factors. Equation (28) defines the amount of curtailed renewable energy in area n.

$$0 \leqslant P_{n,s,t}^{w} \leqslant \left(S_{n,w}^{0} + S_{n,w}^{LA}\right) U_{n,s,t}^{w}, \tag{26}$$

$$0 \leqslant P_{n,s,t}^{pv} \leqslant \left(S_{n,pv}^{0} + S_{n,pv}^{LA}\right) U_{n,s,t}^{pv}, \tag{27}$$

$$P_{n}^{cur,LA} = \sum_{s\in\Omega_s}\sum_{t\in\Omega_T}\left[\left(S_{n,w}^{0} + S_{n,w}^{LA}\right) U_{n,s,t}^{w} + \left(S_{n,pv}^{0} + S_{n,pv}^{LA}\right) U_{n,s,t}^{pv} - P_{n,s,t}^{w} - P_{n,s,t}^{pv}\right], \tag{28}$$

4. Solution Methodology

4.1. Distributed Coordination Solution Based on ATC

The ATC algorithm is a widely adopted distributed solving technique. The fundamental idea of this algorithm is to design the optimization objectives across multiple levels: the system level and the subsystem level [27]. The objectives are assigned from the top down, whereas the responses are continuously provided from the bottom up. Problems at both the system and subsystem levels are optimized independently through an alternating iterative process until convergence is achieved. This method has a rigorous convergence proof and is particularly effective for large-scale, multilevel system optimization challenges [28,29].

The ATC algorithm is applied to address hierarchical coordinated planning problems in this paper. Within this framework, the SW planning model handles system-level tasks and the LA planning model handles subsystem tasks. The consistency constraints of coupling variables are introduced as follows:

$$\begin{cases} S_{n,r}^{SW} = S_{n,r}^{LA} \\ P_{n,s,t}^{SW} = P_{n,s,t}^{LA} \\ P_{n}^{cur,SW} = P_{n}^{cur,LA} \end{cases}, \tag{29}$$

According to the ATC algorithm, Equation (29) is relaxed through Lagrangian relaxation and penalty functions [30], allowing it to be integrated into the objective functions. Consequently, the objective functions presented in Equations (4) and (16) can be reformulated as follows:

$$\begin{aligned} F^{SW} = \min_{\substack{S_{n,w}^{SW}, S_{n,pv}^{SW}, S_{n,ESS}^{SW} \\ P_{n}^{cur,SW}, P_{s,t}^{buy}, P_{n,s,t}^{SW}}} & \sum_{n\in\Omega_n}\sum_{r\in\Omega_r} B_{n,r} S_{n,r}^{SW} \frac{\vartheta(1+\vartheta)^{Y^r}}{(1+\vartheta)^{Y^r}-1} + \sigma \sum_{n\in\Omega_n} \lambda^{cur} P_{n}^{cur,SW} \\ & + \sigma\left[\sum_{n\in\Omega_n}\sum_{s\in\Omega_s}\sum_{t\in\Omega_T} p_{s}^{0}\left(\lambda^{trans} P_{n,s,t}^{SW}\right) + \sum_{s\in\Omega_s}\sum_{t\in\Omega_T} p_{s}^{0}\left(\lambda^{buy} P_{s,t}^{buy} - \lambda^{sell} P_{s,t}^{sell}\right)\right] \\ & + \sum_{n\in\Omega_n}\sum_{r\in\Phi_r}\left[\begin{array}{c} v_{n,r}\left(S_{n,r}^{SW} - S_{n,r}^{LA}\right) \\ \omega_{n,r}\left(S_{n,r}^{SW} - S_{n,r}^{LA}\right)^2 \end{array}\right] + \sum_{n\in\Omega_n}\sum_{s\in\Phi_s}\sum_{t\in\Omega_T}\left[\begin{array}{c} v_{n,s,t}\left(P_{n,s,t}^{SW} - P_{n,s,t}^{LA}\right) \\ \omega_{n,s,t}\left(P_{n,s,t}^{SW} - P_{n,s,t}^{LA}\right)^2 \end{array}\right] \\ & + \sum_{n\in\Omega_n}\left[\begin{array}{c} v_{n}^{cur}\left(P_{n}^{cur,SW} - P_{n}^{cur,LA}\right) \\ \omega_{n}^{cur}\left(P_{n}^{cur,SW} - P_{n}^{cur,LA}\right)^2 \end{array}\right] \end{aligned}, \tag{30}$$

$$
\begin{aligned}
F_n^{LA} = & \min_{\substack{S_{n,r}^{LA},\, P_n^{cur,LA} \\ P_{n,s,t}^{LA},\, e_{n,s,t}^{dis},\, e_{n,s,t}^{ch}}} \sum_{r\in\Phi_r} \begin{bmatrix} v_{n,r}\left(S_{n,r}^{LA} - S_{n,r}^{SW}\right) \\ \omega_{n,r}\left(S_{n,r}^{LA} - S_{n,r}^{SW}\right)^2 \end{bmatrix} \\
& + \sum_{t\in\Omega_t}\sum_{s\in\Omega_s} \begin{bmatrix} v_{n,s,t}\left(P_{n,s,t}^{LA} - P_{n,s,t}^{SW}\right) \\ \omega_{n,s,t}\left(P_{n,s,t}^{LA} - P_{n,s,t}^{SW}\right)^2 \end{bmatrix} + \sum_{n\in\Omega_n} \begin{bmatrix} v_n^{cur}\left(P_n^{cur,LA} - P_n^{cur,SW}\right) \\ \omega_n^{cur}\left(P_n^{cur,LA} - P_n^{cur,SW}\right)^2 \end{bmatrix} \\
& + \max_{\substack{\widetilde{p}_{n,s}^{D},\, \widetilde{P}_{n,s}^{g\max} \\ \widetilde{P}_{n,s}^{g\min}}} \min_{\substack{P_{n,s,t}^{g},\, P_{n,s,t}^{w},\, P_{n,s,t}^{pv} \\ P_{n,s,t}^{dis},\, P_{n,s,t}^{ch},\, E_{n,s,t}^{ESS}}} \sigma \sum_{s\in\Omega_s}\sum_{t\in\Omega_T} p_s^0 \begin{bmatrix} f\left(P_{n,s,t}^{g}\right) + c^{bt}\left(P_{n,s,t}^{dis} + P_{n,s,t}^{ch}\right) \\ +\lambda^{cur} P_{k,s}^{w} + \lambda^{cur} P_{k,s}^{pv} \end{bmatrix}
\end{aligned}
\tag{31}
$$

where $v_{n,r}$, $v_{n,s,t}$, and v_n^{cur} are Lagrangian multipliers; $\omega_{n,r}$, $\omega_{n,s,t}$, and ω_n^{cur} are penalty parameters. It should be noted that $S_{n,r}^{LA}$, $P_{n,s,t}^{LA}$, and $P_n^{cur,LA}$ are constant with respect to the SW planning model, while $S_{n,r}^{SW}$, $P_{n,s,t}^{SW}$, and $P_n^{cur,SW}$ are constant with respect to the LA planning model.

The solution process for the ATC algorithm is outlined below, and the flowchart illustrating the ATC algorithm is presented in Figure 2.

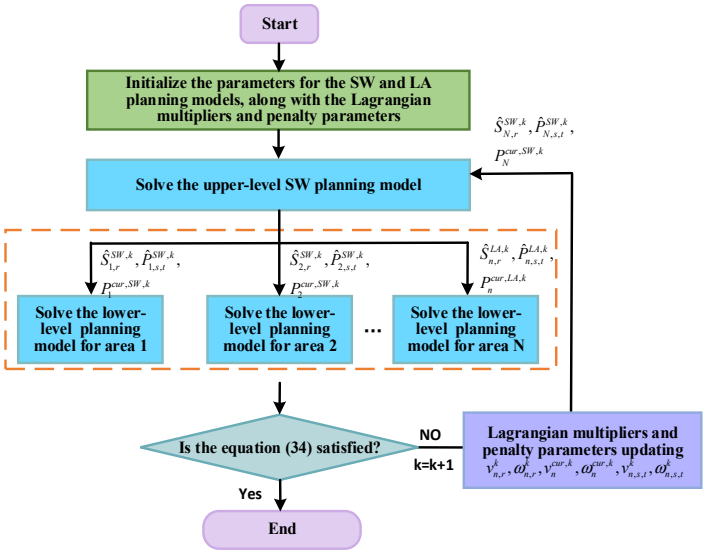


Figure 2. The solution procedure of ATC algorithm.

Step 1: Load the input data. The investment and operational data of the SW and LA system are imported, and information about the uncertainties is incorporated into the model.

Step 2: Initialize the parameters. Set the iteration index $k = 0$. Initialize the coupled parameters $S_{n,r}^{SW,k}$, $P_{n,s,t}^{SW,k}$, $P_n^{cur,SW,k}$, $S_{n,r}^{LA,k}$, $P_{n,r}^{LA,k}$, and $P_n^{cur,LA,k}$. Initialize the Lagrangian and penalty multipliers $v_{n,r}^k$, $\omega_{n,r}^k$, $v_n^{cur,k}$, $\omega_n^{cur,k}$, $v_{n,s,t}^k$, and $\omega_{n,s,t}^k$ for the penalty function's linear and quadratic terms.

Step 3: Problem computation. Standard solvers for mixed-integer quadratic programming (MIQP) are used to solve the SW planning problem with the parameters $S_{n,r}^{LA,k}$, $P_{n,r}^{LA,k}$, and $P_n^{cur,LA,k}$ to obtain the optimal solution x_{k+1}. Solve the n-th LA planning problem with the parameters $S_{n,r}^{SW,k}$, $P_{n,s,t}^{SW,k}$, and $P_n^{cur,SW,k}$ to determine the optimal solution z_{k+1} using the C&CG algorithm. Update the optimal solutions, as follows:

$$x_{k+1} = x_k + \tau(x_{k+1} - x_k), \tag{32}$$

$$z_{k+1} = z_k + \tau(z_{k+1} - z_k), \tag{33}$$

where $x = \left\{S_{n,r}^{SW,k+1}, P_{n,s,t}^{SW,k+1}, P_n^{cur,SW,k+1}\right\}$ represents the coupled parameters in the SW planning problem; and $z = \left\{S_{n,r}^{LA,k+1}, P_{n,s,t}^{LA,k+1}, P_n^{cur,LA,k+1}\right\}$ represents the coupled parameters in the n-th LA planning problem.

Step 4: Convergence check. If the condition in Equation (34) is satisfied, terminate calculation and return the optimal solution.

$$\begin{cases} \left|P_{n,s,t}^{LA,k} - P_{n,s,t}^{SW,k}\right| + \left|S_{n,r}^{LA,k} - S_{n,r}^{SW,k}\right| + \left|P_n^{cur,LA,k} - P_n^{cur,SW,k}\right| \leqslant \varepsilon_1 \\ \dfrac{\left|F^{SW,k} + \sum\limits_{n\in\Omega_n} F_n^{LA,k} - \left(F^{SW,k-1} + \sum\limits_{n\in\Omega_n} F_n^{LA,k-1}\right)\right|}{\left|F^{SW,k} + \sum\limits_{n\in\Omega_n} F_n^{LA,k}\right| + 1} < \varepsilon_2 \end{cases}, \tag{34}$$

where ε_1 and ε_2 denote convergence criteria, where the former ensures accuracy when optimizing coupling variables independently, and the latter serves as the overall benefit convergence criterion. Otherwise go to Step 5.

Step 5: Multiplier updating. Update the Lagrangian and penalty multipliers for the penalty function's linear and quadratic terms according to Equations (31) and (32), and then go to Step 3 to iterate the process.

$$\begin{cases} v_{n,r}^{k+1} = v_{n,r}^k + 2\omega_{n,r}^k \omega_{n,r}^k \left(S_{n,r}^{WR,k} - S_{n,r}^{SR,k}\right) \\ \omega_{n,r}^{k+1} = \begin{cases} \omega_{n,r}^k, if\left(S_{n,r}^{WR,k} - S_{n,r}^{SR,k}\right) \leqslant \gamma\left(S_{n,r}^{WR,k-1} - S_{n,r}^{SR,k-1}\right), \\ \beta\omega_{n,r}^k, otherwise \end{cases} \end{cases} \tag{35}$$

$$\begin{cases} v_{n,s,t}^{k+1} = v_{n,s,t}^k + 2\omega_{n,s,t}^k \omega_{n,s,t}^k \left(P_{n,s,t}^{sa,k} - P_{n,s,t}^{wa,k}\right) \\ \omega_{n,s,t}^{k+1} = \begin{cases} \omega_{n,s,t}^k, if\left(P_{n,s,t}^{sa,k} - P_{n,s,t}^{wa,k}\right) \leqslant \gamma\left(P_{n,s,t}^{sa,k-1} - P_{n,s,t}^{wa,k-1}\right). \\ \beta\omega_{n,s,t}^k, otherwise \end{cases} \end{cases} \tag{36}$$

$$\begin{cases} v_n^{cur,k+1} = v_n^{cur,k} + 2\omega_n^{cur,k} \omega_n^{cur,k} \left(P_n^{cur,WR,k} - P_n^{cur,SR,k}\right) \\ \omega_n^{cur,k+1} = \begin{cases} \omega_n^{cur,k}, if\left(P_n^{cur,WR,k} - P_n^{cur,SR,k}\right) \leqslant \gamma\left(P_n^{cur,WR,k-1} - P_n^{cur,SR,k-1}\right), \\ \beta\omega_{n,s,t}^k, otherwise \end{cases} \end{cases} \tag{37}$$

4.2. C&CG Algorithm for the LA Planning Problem Under Uncertainty

In the paper, Equation [31] is reformulated based on a stochastic adaptive robust optimization approach to handle uncertainties [4]. The reformulated objective function features a three-level structure:

1. Capacity decision (Level 1): Determine capacity decisions that minimize deviations from the SW planning outcomes.
2. Worst-case scenario (Level 2): Following the establishment of capacity decisions, assess the worst-case scenarios of uncertain future peak demands and the output boundaries of thermal plants.
3. Corrective actions (Level 3): Once the capacity decisions are made and the worst-case scenarios are realized, corrective actions are taken to minimize operational costs.

The accuracy of the LA planning model for individual areas directly affects the solution process of the hierarchical coordination planning problem. However, the inherent multilevel structure can easily result in NP-hard problems, complicating direct solutions. The C&CG algorithm, as introduced in [31], can effectively solve these difficulties. This algorithm has proven to improve computational efficiency and solution reliability for two-stage robust optimization problems in power and energy systems [32–34]. To reduce

computational complexity, the C&CG algorithm is applied to solve the three-level structure for the individual area.

In accordance with the C&CG algorithm, the three-level optimization problem can be decomposed into a master problem and a subproblem, which are iteratively solved until convergence. For a given $\left\{S_{n,r}^{LA*}, P_{n}^{cur,LA*}, P_{n,s,t}^{LA*}, e_{n,s,t}^{dis*}, e_{n,s,t}^{ch*}\right\}$ obtained from the master problem at each iteration, the subproblem associated with Equation (31) can be described by the following:

$$(\mathcal{SP}-n): \max_{\substack{\widetilde{p}_{n,s}^{D},\widetilde{P}_{n,s}^{g\max},\\ \widetilde{P}_{n,s}^{g\min}}} \min_{\substack{P_{n,s,t}^{g},P_{n,s,t}^{w},P_{n,s,t}^{pv},\\ P_{n,s,t}^{dis},P_{n,s,t}^{ch},E_{n,s,t}^{ESS}}} \sigma \sum_{s\in\Omega_s}\sum_{t\in\Omega_T} \rho_s \left[\begin{array}{l} f\left(P_{n,s,t}^{g}\right)+c^{bt}(P_{n,s,t}^{dis}+P_{n,s,t}^{ch}) \\ +\lambda^{w}P_{k,s}^{w}+\lambda^{w}P_{k,s}^{pv} \end{array}\right], \tag{38}$$

The compact matrix formulation of subproblem is described as follows:

$$\max_{\boldsymbol{d}\in\mathbf{D}} \min_{\boldsymbol{y}\in\boldsymbol{\Omega}(\boldsymbol{x}^*,\boldsymbol{d})} \boldsymbol{b}^{\mathrm{T}}\boldsymbol{y}, \tag{39}$$

$$\text{s.t. } \boldsymbol{A}\boldsymbol{y}+\boldsymbol{B}\boldsymbol{d}+\boldsymbol{C}\boldsymbol{x}^*=\boldsymbol{g}, \tag{40}$$

$$\boldsymbol{D}\boldsymbol{x}^*+\boldsymbol{E}\boldsymbol{y}+\boldsymbol{F}\boldsymbol{d}\leqslant\boldsymbol{h}, \tag{41}$$

where $\boldsymbol{x}^* = \left\{S_{n,r}^{LA*}, P_{n}^{cur,LA*}, P_{n,s,t}^{LA*}, e_{n,s,t}^{dis*}, e_{n,s,t}^{ch*}\right\}$ denotes the first-stage decision obtained from the master problem; $\boldsymbol{y} = \left\{P_{n,s,t}^{g}, P_{n,s,t}^{w}, P_{n,s,t}^{PV}, P_{n,s,t}^{dis}, P_{n,s,t}^{ch}, E_{n,s,t}^{ESS}\right\}$ denotes the second-stage decision variables; and $\boldsymbol{d} = \left\{\widetilde{p}_{n,s}^{D}, \widetilde{P}_{n,s}^{g\max}, \widetilde{P}_{n,s}^{g\min}\right\}$ indicates the uncertain variables defined by the uncertainty set $\boldsymbol{D}$. Equation (41) gathers the equality constraints from Equations (18) and (21), while Equation (42) compiles the inequality constraints from Equations (19), (20), (22) and (29).

The Karush–Kuhn–Tucker (KKT) conditions are utilized to transform the subproblem into a single-level problem [35,36].

$$\max_{\substack{\boldsymbol{d}\in\mathbf{D}\\ \boldsymbol{y}\in\boldsymbol{\Omega}(\boldsymbol{x}^*,\boldsymbol{d})\\ \boldsymbol{\lambda},\boldsymbol{\mu},\boldsymbol{\omega}}} \boldsymbol{b}^{\mathrm{T}}\boldsymbol{y}, \tag{42}$$

$$\text{s.t. (40)–(41)}, \tag{43}$$

$$\boldsymbol{A}^{\mathrm{T}}\boldsymbol{\mu}+\boldsymbol{E}^{\mathrm{T}}\boldsymbol{\omega}=\boldsymbol{b}, \tag{44}$$

$$(\boldsymbol{D}\boldsymbol{x}^*+\boldsymbol{E}\boldsymbol{y}+\boldsymbol{F}\boldsymbol{d}-\boldsymbol{h})_p\omega_p=0,\ \ \forall p, \tag{45}$$

$$\left(\boldsymbol{A}^{\mathrm{T}}\boldsymbol{\mu}+\boldsymbol{F}^{\mathrm{T}}\boldsymbol{\omega}-\boldsymbol{b}\right)_q y_q=0,\ \ \forall q, \tag{46}$$

$$\boldsymbol{\omega}\leqslant 0, \boldsymbol{\mu} \text{ is free }, \tag{47}$$

where $\boldsymbol{\omega}, \boldsymbol{\mu}$ are dual variables for (40) and (41), respectively, and p, q are indices of constraints and variables. Equations (45) and (46) represent complementary slackness conditions that are nonlinear, which can be linearized on the basis of the big-M method. For example, Equation (45) can be reformulated in the following manner:

$$\omega_p\geqslant-\epsilon_p M, (\boldsymbol{D}\boldsymbol{x}^*+\boldsymbol{E}\boldsymbol{y}+\boldsymbol{F}\boldsymbol{d}-\boldsymbol{h})_p\geqslant-(1-\epsilon_p)M, \epsilon_p\in\{0,1\}, \tag{48}$$

where ϵ_p is a binary variable. If $\epsilon_p = 0$, then $\omega_p = 0$ and $\boldsymbol{D}\boldsymbol{x}^*+\boldsymbol{E}\boldsymbol{y}+\boldsymbol{F}\boldsymbol{d}\leq\boldsymbol{h}$, else if $\epsilon_p = 1$, then $\omega_p\leq 0$ and $\boldsymbol{D}\boldsymbol{x}^*+\boldsymbol{E}\boldsymbol{y}+\boldsymbol{F}\boldsymbol{d}=\boldsymbol{h}$. Therefore, Equation (48) is equivalent to Equation (45).

As a result, the subproblem is converted into a mixed-integer linear programming (MILP) format, which can be effectively addressed using MILP solvers.

For a given $\left\{\widetilde{P}^{D*}_{n,s}, \widetilde{P}^{g\max*}_{n,s}, \widetilde{P}^{g\min*}_{n,s}\right\}$ obtained from the subproblem, the master problem can be formulated as follows:

$$\min_{\substack{S^{SR}_{n,w}, S^{SR}_{n,pv}, S^{SR}_{n,ESS}, \\ P^{cur,SR}_{n}, P^{SR}_{n,s,t}, e^{dis}_{n,s,t}, e^{ch}_{n,s,t}}} \sum_{r\in\Phi_r}\begin{bmatrix} v_{n,r}\left(S^{LA}_{n,r}-S^{SW}_{n,r}\right) \\ \omega_{n,r}\left(S^{LA}_{n,r}-S^{SW}_{n,r}\right)^2 \end{bmatrix} + \sum_{t\in\Omega_t}\sum_{s\in\Omega_s}\begin{bmatrix} v_{n,s,t}\left(P^{LA}_{n,s,t}-P^{SW}_{n,s,t}\right) \\ \omega_{n,s,t}\left(P^{LA}_{n,s,t}-P^{SW}_{n,s,t}\right)^2 \end{bmatrix} + \sum_{n\in\Omega_n}\begin{bmatrix} v^{cur}_{n}\left(P^{cur,LA}_{n}-P^{cur,SW}_{n}\right) \\ \omega^{cur}_{n}\left(P^{cur,LA}_{n}-P^{cur,SW}_{n}\right)^2 \end{bmatrix} + \eta, \tag{49}$$

$$\text{s. t. } \eta \geqslant \sigma \sum_{s\in\Omega_s}\sum_{t\in\Omega_T} p^0_s \begin{bmatrix} f\left(P^{g,m}_{n,s,t}\right) + c^{bt}\left(P^{dis,m}_{n,s,t}+P^{ch,m}_{n,s,t}\right) \\ +\lambda^{w}P^{w,m}_{k,s}+\lambda^{PV}P^{PV,m}_{k,s} \end{bmatrix}, \tag{50}$$

$$\widetilde{p}^{D*}_{n,s,m}U^{load}_{n,s,t} = P^{g}_{n,s,t} + P^{w}_{n,s,t} + P^{pv}_{n,s,t} - P^{ch}_{n,s,t} + P^{dis}_{n,s,t} + P^{SR}_{n,s,line}, \tag{51}$$

$$\widetilde{P}^{g\min,m*}_{n,s} \leqslant P^{g}_{n,s,t} \leqslant \widetilde{P}^{g\max,m*}_{n,s}, \tag{52}$$

$$\text{Equations (5)–(7), (13) and (19)–(28)} \tag{53}$$

where m is the iteration index; and η is the auxiliary variable to represent the subproblem.

Based on the C&CG algorithm, the solution procedure of the lower-level LA planning model is described below. The flow chart of C&CG algorithm is shown in Figure 3.

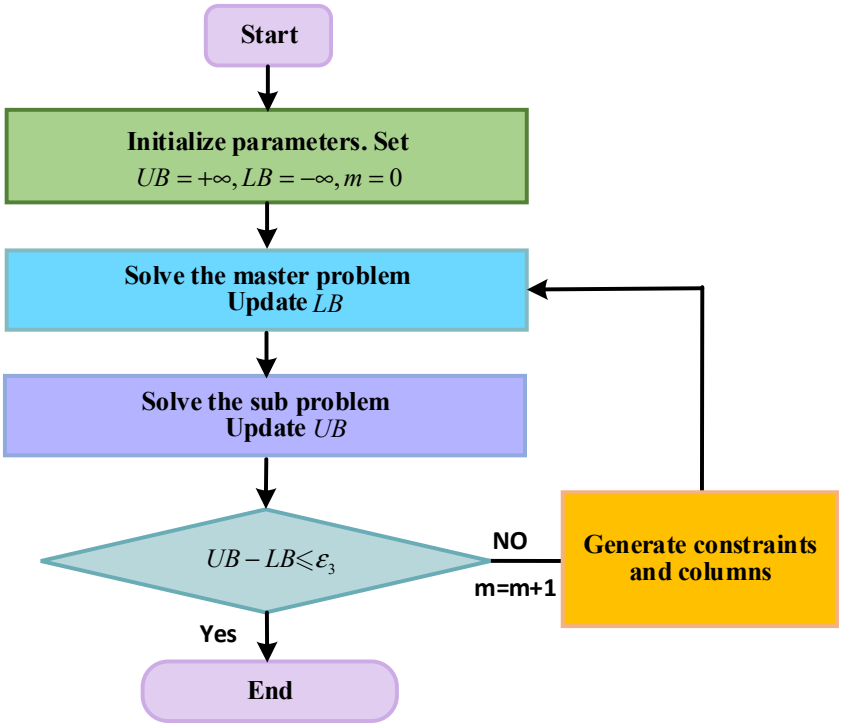


Figure 3. The solution procedure of C&CG algorithm.

Step 1: Initialize the parameters. Set $LB = -\infty$, and $UB = +\infty$. $UB = +\infty$, $LB = -\infty$, $m = 0$ UB LB.

Step 2: Solve the master problem. If $m = 0$, solve the master problem with subject to constraints (50)–(52). Otherwise, solve the complete version of the master problem. Derive the optimal solution $\left\{S^{LA*}_{n,r,m+1}, P^{cur,LA*}_{n,m+1}, P^{LA*}_{n,s,t,m+1}, e^{dis*}_{n,s,t,m+1}, e^{ch*}_{n,s,t,m+1}, \eta^{*}_{m+1}\right\}$. Update

$$LB = \sum_{r\in\Phi_r}\begin{bmatrix} v_{n,r}\left(S^{LA*}_{n,r,m+1} - S^{SW,k}_{n,r,m+1}\right) \\ +\omega_{n,r}\left(S^{LA*}_{n,r,m+1} - S^{SW,k}_{n,r,m+1}\right)^2 \end{bmatrix} + \sum_{t\in\Omega_t}\sum_{s\in\Omega_s}\begin{bmatrix} v_{n,s,t}\left(P^{LA*}_{n,s,t,m+1} - P^{SW,k}_{n,s,t,m+1}\right) \\ +\omega_{n,s,t}\left(P^{LA*}_{n,s,t,m+1} - P^{SW,k}_{n,s,t,m+1}\right)^2 \end{bmatrix} + \sum_{n\in\Omega_n}\begin{bmatrix} v^{cur}_{n}\left(P^{cur,WR,k}_{n} - P^{cur,SR*}_{n,m+1}\right) \\ \omega^{cur}_{n}\left(P^{cur,WR,k}_{n} - P^{cur,SR*}_{n,m+1}\right)^2 \end{bmatrix} + \eta^{*}_{,m+1}.$$

Step 3: Solve the subproblem.

For a given $\left\{S^{LA*}_{n,r,m+1}, P^{cur,LA*}_{n,m+1}, P^{LA*}_{n,s,t,m+1}, e^{dis*}_{n,s,t,m+1}, e^{ch*}_{n,s,t,m+1}, \eta^{*}_{m+1}\right\}$, obtain the optimal solution $\left\{P^{g*}_{n,s,t,m}, P^{w*}_{n,s,t,m}, P^{pv*}_{n,s,t,m}, P^{dis*}_{n,s,t,m}, P^{ch*}_{n,s,t,m}, E^{ESS*}_{n,s,t,m}, \widetilde{P}^{D*}_{n,s,m}, \widetilde{P}^{g\max*}_{n,s,m}, \widetilde{P}^{g\min*}_{n,s,m}\right\}$.

Update $UB = \min\left\{UB, \sigma\sum_{s\in\Omega_s}\sum_{t\in\Omega_T}\rho_s\begin{bmatrix} f\left(P^{g*}_{n,s,t,m}\right) + c^{bt}(P^{dis*}_{n,s,t,m} + P^{ch*}_{n,s,t,m}) \\ +\lambda^{w}P^{w*}_{k,s,m} + \lambda^{w}P^{PV*}_{k,s,m} \end{bmatrix}\right\}$.

Step 4: Check the convergence. If the condition,

$$UB - LB \leqslant \varepsilon_3, \tag{54}$$

is satisfied, the calculation is stopped, and the results are returned. Otherwise, introduce new variables $\left\{P^{g}_{n,s,t,m+1}, P^{w}_{n,s,t,m+1}, P^{pv}_{n,s,t,m+1}, P^{dis}_{n,s,t,m+1}, P^{ch}_{n,s,t,m+1}, E^{ESS}_{n,s,t,m+1}\right\}$ and incorporate the following constraints to the master problem.

$$\eta \geq \sigma\sum_{s\in\Omega_s}\sum_{t\in\Omega_T}\rho_s\begin{bmatrix} f\left(P^{g*}_{n,s,t,m+1}\right) + c^{bt}(P^{dis*}_{n,s,t,m+1} + P^{ch*}_{n,s,t,m+1}) \\ +\lambda^{w}P^{w*}_{k,s,m+1} + \lambda^{w}P^{PV*}_{k,s,m+1} \end{bmatrix} \tag{55}$$

$$\widetilde{P}^{g\min*}_{n,s,m+1} \leqslant P^{g}_{n,s,t} \leqslant \widetilde{P}^{g\max*}_{n,s,m+1}. \tag{56}$$

$$\widetilde{p}^{D*}_{n,s,m+1}U^{load}_{n,s,t} = P^{g}_{n,s,t} + P^{w}_{n,s,t} + P^{pv}_{n,s,t} - P^{ch}_{n,s,t} + P^{dis}_{n,s,t} + P^{SR}_{n,s,line}. \tag{57}$$

Set $m = m + 1$ and go to Step 2.

4.3. Integrated Solution Framework

The ATC algorithm is applied to decouple the upper SW planning problem and the lower LA operational optimization problem in this paper. However, the lower-level LA operational optimization problem, derived from the stochastic adaptive robust optimization model, exhibits a complex multilevel structure that poses significant challenges for resolution. To overcome these difficulties, this section introduces an integrated solution framework that combines ATC and the C&CG algorithm, which is designed to simplify the solution process and improve computational efficiency.

The integrated solution framework, which combines the ATC method with the C&CG algorithm, is depicted in Figure 4. This framework manages the interaction between the upper-level SW planning problem and the lower-level LA planning problem. The coupled variables include the planning capacities for RESs and ESSs, as well as the power injections and renewable energy curtailment for each area under typical scenarios. The ATC algorithm is employed to decouple these problems, updating the relevant variables with each iteration. Specifically, the SW planning problem is addressed using MIQP solvers, while the lower-level LA planning problem, which has higher computational complexity, is tackled using the C&CG algorithm. This approach ensures a robust and distributed planning for multiarea wind-solar-energy storage systems. It is important to note that the combination of ATC and the C&CG algorithms introduces multiple layers and iterative processes, resulting in a complex structure. This complexity can pose challenges in implementation, but it is essential for achieving comprehensive and effective solutions.

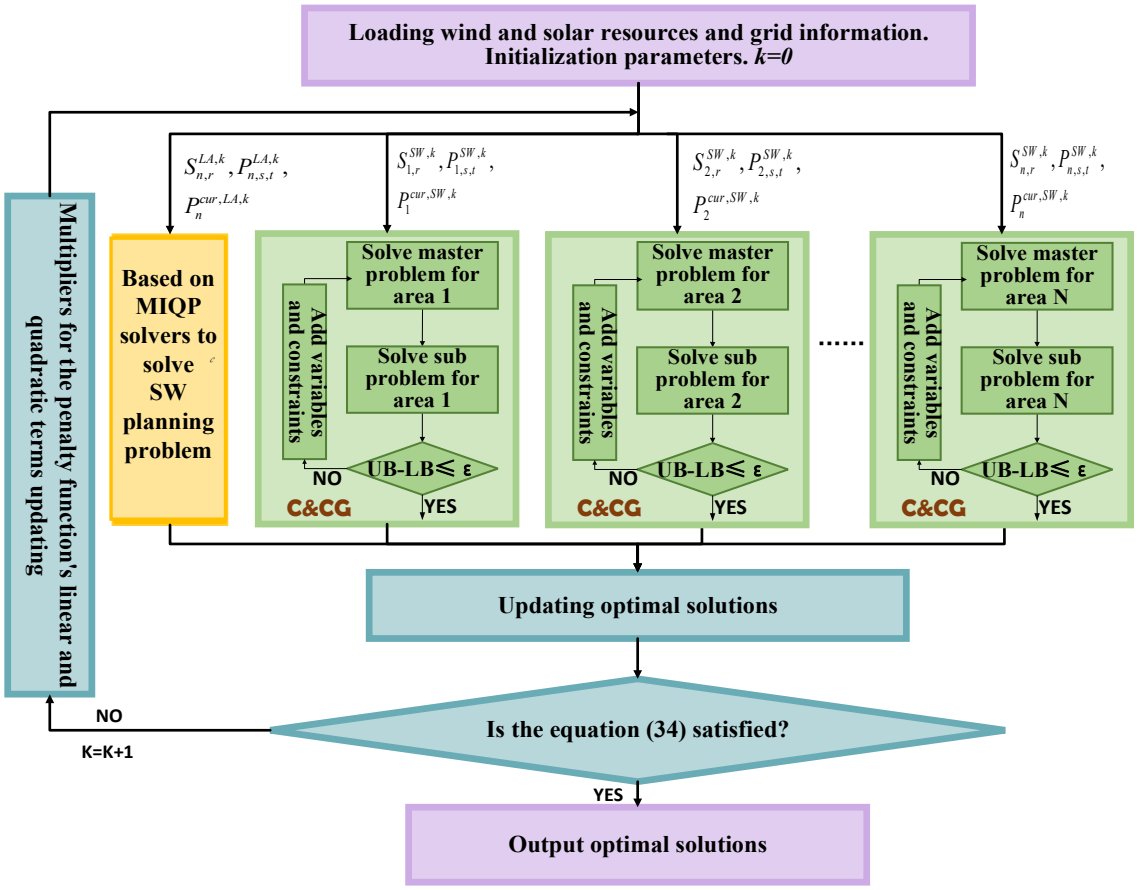


Figure 4. The integrated solution framework combining ATC and the C&CG algorithms.

5. Case Study

This section presents a comprehensive set of numerical results to evaluate the performance of the coordinated planning of multiarea wind-solar-energy storage systems under various sources of uncertainty. It is organized into three parts: (1) description of operational conditions; (2) comparison of coordinated versus independent planning; and (3) analysis of planning under different uncertainty budgets.

5.1. Case Introduction

This section analyzes a case study using actual parameters from an electric grid in a specific Chinese region, which consists of three interconnected areas. The parameters associated with each local area are shown in Table A1. Four representative scenarios were generated, each illustrating the variability and correlations between the demand factors and renewable energy source (RES) capacity factors. These scenarios reflected distinct operational conditions across the four seasons: Scenario 1 corresponds to spring, Scenario 2 corresponds to summer, Scenario 3 corresponds to autumn, and Scenario 4 corresponds to winter. It was noted that the number of scenarios can be easily adjusted to balance computational efficiency with model accuracy. The variations in the demand factors and RES capacity factors for Area 1 are illustrated in Figure 5, whereas the corresponding data for Area 2 are presented in Figure 6. The factors exhibited varying trends, and the evolution trends in these factors differed across different areas within the same scenario. The probabilities of these four typical scenarios were 0.221, 0.286, 0.279, and 0.213, respectively, as determined through the clustering process. The electricity price was set to 0.119 \$/kWh, reflecting the actual electricity price in China. Based on real statistical data from the power grid, the charging and discharging rates of ESSs were set to 0.95 and 0.98, and $\mu_{\min}^{ESS}$ and $\mu_{\max}^{ESS}$ were set to 0.1 and 0.9, respectively.

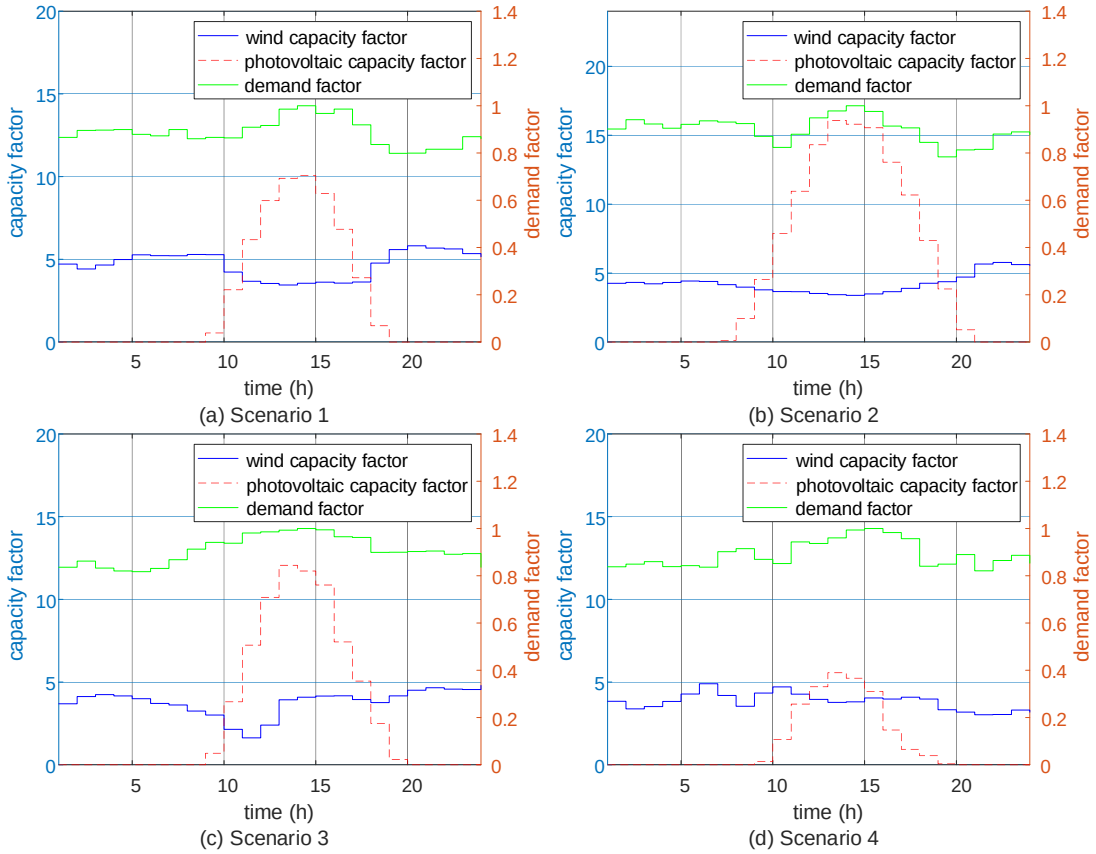


Figure 5. The demand factor and RES capacity factor variations for Area 1.

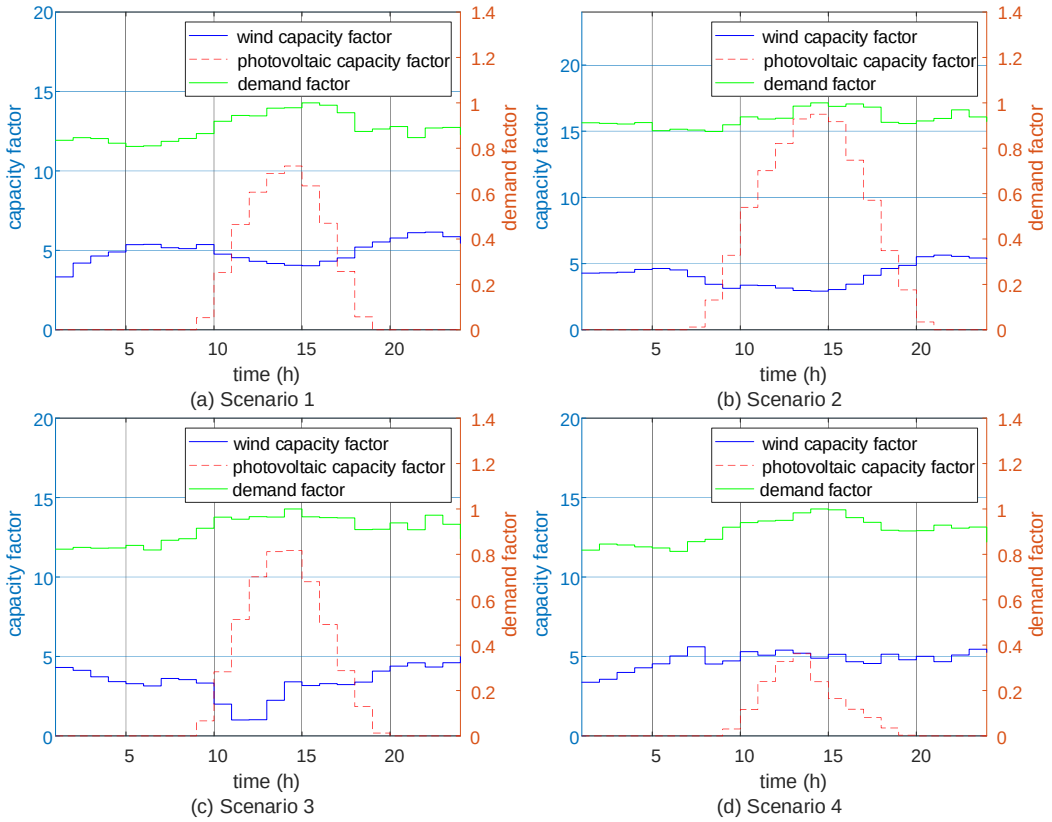


Figure 6. The demand factor and RES capacity factor variations for Area 2.

The initial values for $v_{n,s,t}$ and v_n^{cur} were set to 0.028 \$/kWh, which was chosen to be lower than the electricity price. The initial values of $\omega_{n,s,t}$ and ω_n^{cur} were set to 0.112 \$/kWh. The initial values for $v_{n,r}$ and $\omega_{n,r}$ were set to 14 and 19.8 \$/kWh, respectively. It is important to note that, in contrast to the Lagrangian multipliers $v_{n,s,t}$, v_n^{cur}, and $v_{n,r}$, the penalty parameters $\omega_{n,s,t}$, ω_n^{cur}, and $\omega_{n,r}$ significantly influence the convergence of the algorithm. Thus, they were determined using the trial-and-error methods as described in [37,38]. To achieve an optimal balance between convergence rate and solution accuracy, the parameters τ and ε were set to small values of 0.9 and 10^{-2}, respectively. Furthermore, we considered that the peak demand and the output boundaries of thermal plants might vary by 10% and 20% from their predicted values, respectively.

The model was constructed in the MATLAB R2023b environment using the YALMIP R20230609 toolkit and was solved using the Gourbi solver.

5.2. Comparison of Coordinated and Independent Planning Method

To validate the economic and effective benefits of considering regional cooperation in capacity configuration, we compared the coordinated planning model proposed in this paper with an independent planning model. This section presents two different planning cases for comparative analysis.

Case 1: the proposed hierarchical coordinated planning model, which integrates regional cooperation and interconnections.

Case 2: the independent model, which optimizes each area in isolation without considering regional interconnections.

The installed capacities of RESs and ESSs in different cases are shown in Figure 7. Notably, the installed capacities for wind, solar, and storage were significantly higher for Case 2 than for Case 1. In Case 1, the average proportion of installed ESS capacity was 18%. Conversely, Case 2 showed a substantial increase in the installation rate, reaching 61%. This suggests that a greater share of ESSs is necessary in a power system lacking regional cooperation to effectively manage the intermittency of renewable energy sources.

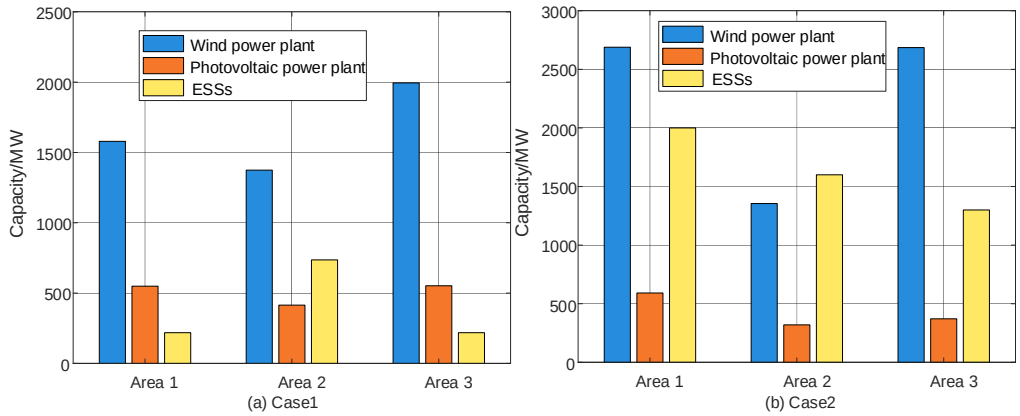


Figure 7. Installed capacities of RESs and ESSs in different cases.

The expected renewable energy curtailment is defined as weighted sum of energy curtailment across all typical scenarios, where each scenario's contribution is multiplied by its probability. Figure 8 shows the expected renewable energy curtailment of RESs and the corresponding curtailment ratios across various areas. The results indicate that the coordinated planning model reduced renewable energy curtailment. In Case 1, the curtailment rate in each area was minimal, remaining below 0.01%. By contrast, Case 2 revealed a marked increase in the curtailment rates across all areas. Specifically, Area 1 experienced a significant curtailment rate of up to 0.3%. This stark difference highlights the impact of the planning method on the efficiency of renewable energy utilization.

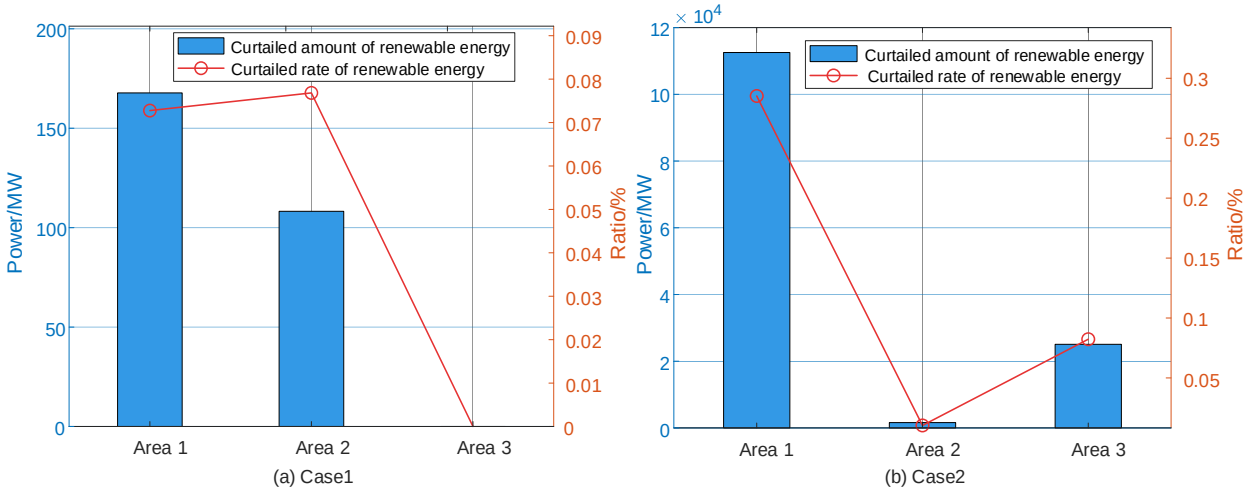


Figure 8. Curtailed electricity of RESs and curtailment ratio for different cases.

Table 1 presents a comparative analysis of the investment and operational costs associated with Cases 1 and 2 across three areas. In Case 1, the investment costs for Areas 1, 2, and 3 are 0.014, 0.024, and 0.016, respectively. The corresponding operational costs for these areas are 0.872, 0.41, and 0.641. It indicates a relatively low initial financial commitment, which may increase attractiveness for planners seeking cost-effective solutions. By contrast, Case 2 presents a markedly different financial profile, characterized by higher investment costs of 0.060, 0.044, and 0.043 for areas 1, 2, and 3, respectively. Moreover, the operational costs in this case are significantly elevated, with values of 2.79, 0.47, and 0.952. This significant increase in costs can be attributed to the independent planning approach, which fails to fully leverage the complementary relationship between power sources and loads across different areas. As a result, this leads to redundant investments in power generation, ultimately undermining the economic efficiency of Case 2.

Table 1. Comparison of costs of different cases.

	Investment Cost ($ Billion)			**Operational Cost ($ Billion)**		
	Area 1	**Area 2**	**Area 3**	**Area 1**	**Area 2**	**Area 3**
Case 1	0.014	0.024	0.016	0.872	0.41	0.641
Case 2	0.06	0.044	0.043	2.79	0.47	0.952

Overall, compared with the independent planning approach, the proposed hierarchical planning approach not only optimizes the deployment of wind, solar, and storage resources but also lowers financial expenditures, leading to a more efficient and cost-effective energy system.

5.3. Coordinated Planning Under Different Budgets of Uncertainty

Each LA planning model contains the frequency of worst-case scenario uncertainties. By adjusting this frequency in the plan-making process, we can control the conservativeness of the optimal plan. The installed capacity of planning schemes under different uncertainty budgets was evaluated, as shown in Figure 9. Specifically, B0, B1, B2, and B3 represent progressively increasing levels of uncertainty budgets, which correspond to $\Gamma = 0$, $\Gamma = 1$, $\Gamma = 2$, and $\Gamma = 3$, respectively. As the uncertainty budgets increased, a notable increase in the installed capacity for renewable energy sources and energy storage systems was observed across the three areas.

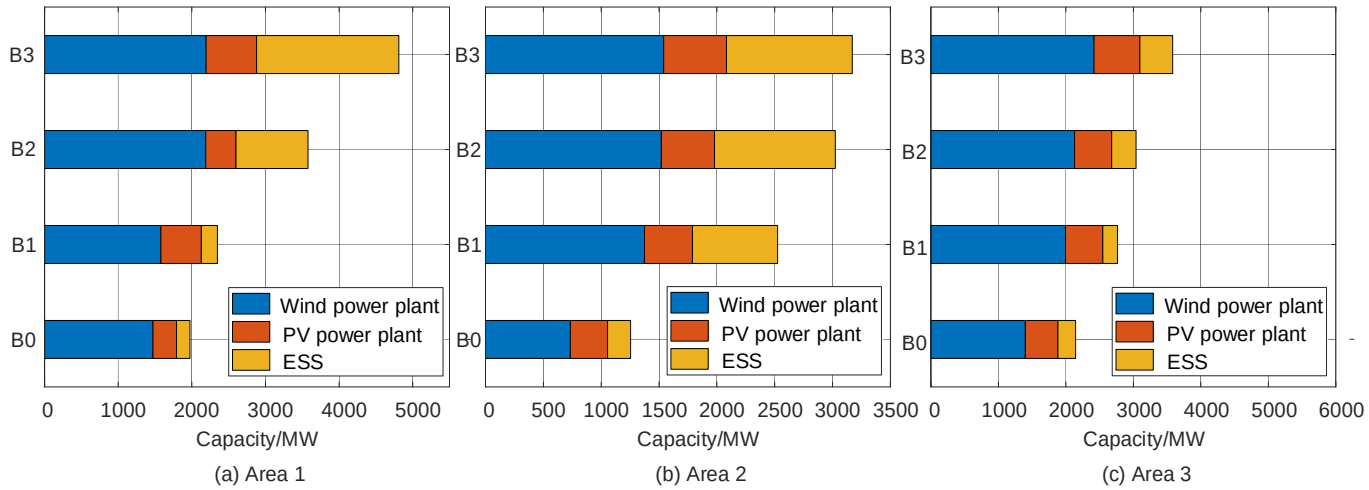


Figure 9. Installed capacities of RESs and ESSs under different uncertainty budgets.

Figure 10 provides insights into the expected amounts of curtailed renewable energy and the associated curtailment rates for the entire system under different uncertainty budgets. As the uncertainty budget grows, both the quantity of curtailed renewable energy and the curtailment rate increase significantly. For example, curtailed renewable energy increases from less than 1000 MW to a rather substantial 15,670 MW, while the curtailment rate increases from below 0.1% to 2.87%.

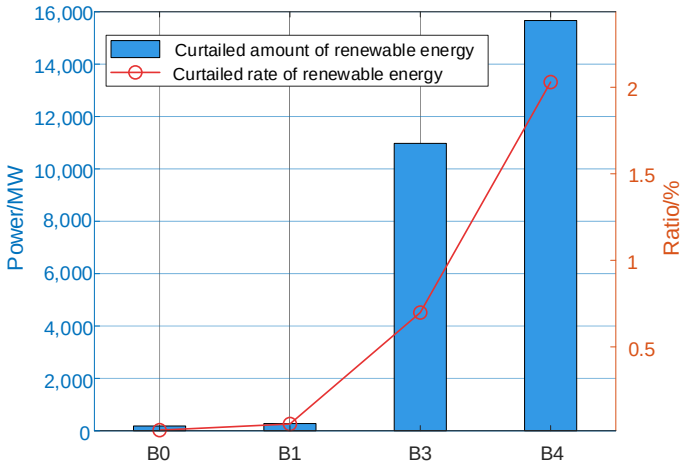


Figure 10. Curtailed electricity of RESs and curtailment ratio for the entire system under different uncertainty budgets.

Figure 11 offers a detailed view of the energy exchange dynamics between the wide-area system and neighboring areas under different uncertainty budgets. Within the same scenario, the energy exchange patterns under different uncertainty budgets clearly exhibited similar trends. As the uncertainty budget increased, there was a substantial rise in the energy exchanged. This trend was consistent across all four considered scenarios.

Table 2 summarizes the investment and operational costs associated with different uncertainty budgets across the three designated regions. The data presented in this table demonstrate clear correlation between the increase in the level of uncertainty and the financial implications for energy planning. As shown in Table 2, the increase in the uncertainty levels directly leads to higher investment costs for each area. For example, in Area 1, the investment cost in the low-uncertainty scenario was 0.011, whereas it increased to 0.056 in the high-uncertainty scenario. Areas 2 and 3 also exhibited corresponding growth trends, emphasizing that planners need to allocate more resources to mitigate unpredictable risks when faced with greater uncertainty. Furthermore, operational expenses also increased

significantly with rising uncertainty. In Area 1, operational costs increased from 0.675 to 0.974, and this pattern was validated across all areas as the uncertainty budget expands. In conclusion, the results presented in Table 2 highlight the critical impact of uncertainty on both investment and operational costs in energy planning. As the level of uncertainty increases, stakeholders face the dual challenge of managing higher upfront investments and ongoing operational expenses. This necessitates a strategic approach to energy planning that balances risk management with cost efficiency, ensuring that energy systems remain resilient and capable of adapting to changing conditions.

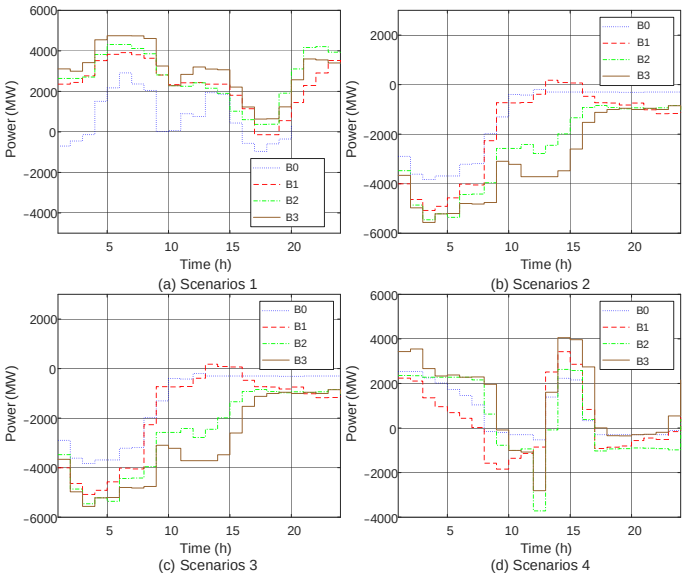


Figure 11. Power exchange with external grid under different uncertainty budgets.

Table 2. Comparison of cost among different uncertainty budgets.

	Investment Cost ($ Billion)			**Operational Cost ($ Billion)**		
	Area 1	**Area 2**	**Area 3**	**Area 1**	**Area 2**	**Area 3**
B0	0.011	0.009	0.014	0675	0.381	0.61
B1	0.014	0.024	0.016	0.872	0.410	0.641
B2	0.034	0.032	0.020	0926	0.422	0.768
B3	0.056	0.033	0.024	0.974	0.432	0.91

5.4. Computational Times

The findings of this case study were derived from a Dell Intel Core i7-12700H processor, sourced from Dell Inc., located in Round Rock, TX, USA, and equipped with 16 GB of RAM. To assess the computational performance of the proposed planning method for large-scale systems, we analyzed multiarea power systems of varying scales. These larger systems were constructed via duplicating the aforementioned wide-system and interconnecting them. Table 3 provides a comprehensive overview of the computational data for large-scale systems consisting of three, six, and nine areas. Remarkably, fewer than 20 iterations between the upper-level and lower-level problems are needed to resolve these complex systems. The number of equations, continuous variables, and binary variables all exhibit an increasing trend as the system scale grows, reflecting an increase in problem complexity. While computational time increases with the system size, the wide-system comprising nine areas remains within a reasonable range, requiring approximately 6893 s. It is important to note that this duration aligns well with the requirements for a planning study. Overall, these results validate the computation effectiveness of the proposed method in handling large-scale system challenges.

Table 3. Computational complexity for multiple areas of different scales.

	Items	3 Areas	6 Areas	9 Areas
SW planning problem	No. of Equations	20	32	44
	No. of Cont. variables	16	31	41
	No. of Bin. variables	0	0	0
LA planning problem	No. of Equations	48	96	144
	No. of Cont. variables	42	84	126
	No. of Bin. variables	6	12	18
Total	No. of Iterations	7	10	15
	Time (s)	5834	6357	6893

6. Discussion

In this study, we developed a coordinated planning method for multiarea wind-solar-energy storage systems that effectively addresses the complexities introduced via various uncertainties. Our proposed framework allows for the simultaneous handling of interarea coordination and multiple uncertainties. While some studies have focused on interarea coordination, they often overlook the intricacies of multiple uncertainties [16–18]. Conversely, others may address uncertainties but fail to consider interarea coordination [13–15]. By integrating these two dimensions, our approach yields results that provide a more realistic perspective on the challenges faced in multiarea systems.

Our comparative analysis with independent planning methods reveals that our hierarchical planning approach not only minimizes redundancy in resource allocation but also significantly lowers overall costs while enhancing the utilization rates of renewable energy sources (RESs). The uneven distribution of renewable energy resources across different regions presents both challenges and opportunities. For example, some areas may be abundant in solar energy, while others may have considerable wind potential. By facilitating power transfers between areas, we can optimize the allocation of these dispersed energy resources, thereby improving overall energy utilization efficiency. As the share of renewable energy increases, certain regions may face generation supply that exceeds demand, leading to underutilization of wind and solar resources (i.e., curtailment). Interarea power transmission can alleviate this issue via redirecting surplus energy to high-demand regions. Consequently, by incorporating interconnection characteristics during the planning stage, we can significantly lower both investment and operational expenditures.

Another key finding of our research is the substantial impact of uncertainty on capital investment decisions. The integration of stochastic programming and robust optimization techniques is essential for accurately modeling these uncertainties. Stochastic programming effectively captures the variability and correlations between demand factors and RES capacity factors using a set of typical scenarios. The robust optimization, based on the confidence bound, facilitates a more resilient planning strategy that adapts to fluctuating energy demands and variable renewable energy outputs. As the uncertainty budget increases, we observed a corresponding rise in investments in wind, solar, and storage capacities, emphasizing the necessity of establishing an appropriate uncertainty budget based on regional resource potentials. This creates a trade-off in terms of techno-economic indices, highlighting the importance of establishing an appropriate uncertainty budget. By carefully balancing these factors, stakeholders can optimize investments while ensuring that the allocation strategy remains resilient in the face of fluctuating conditions.

The results of our study underscore the importance of coordinated planning in optimizing the deployment of renewable energy resources. By integrating both system-wide and local area planning models, we can achieve a more efficient energy system. This approach not only facilitates cost savings but also enhances the utilization of renewable energy, which is crucial for meeting sustainability goals.

7. Conclusions

This paper introduces a coordinated planning method of wind-solar-energy storage systems across multiarea considering multiple uncertainties, which incorporates both system-wide and local area planning model. The SW planning model is designed to optimize investments in the RES and ESS, as well as to determine the operational boundaries of LAs. The LA planning model applies robust optimization techniques and stochastic programming techniques to address multiple uncertainties. It refines operational strategies and further optimizes capacities of RESs and ESSs based on local conditions and specific requirements. The main conclusions are as follows:

(1) In comparison to independent planning, the proposed hierarchical coordinated planning method effectively reduces redundancy in the configuration of wind, solar, and energy storage capacities. Furthermore, it reduces the overall cost by 54.6% and improves the RES utilization rate by 5.6% on average. The coordinated planning method significantly lowers economic costs and improves the utilization of renewable energy sources.

(2) From the perspective of uncertainty management, the proposed method can be controlled to adjust the conservativeness of the allocation strategy solution to address changes in uncertainty. As the uncertainty budget increases, investments in wind, solar, and storage capacities generally rise accordingly, as well as the operational cost. There is a trade-off in terms of techno-economic indices and it is of significance to set a proper uncertainty budget based on regional resource potentials.

(3) The proposed model is computationally feasible for fairly large power systems. Although computational time does increase as the system size grows, the wide-system with nine areas still operates within a reasonable timeframe, taking about 6893 s to compute.

Moreover, while our method effectively achieved economic objectives, the capacity decisions were determined primarily based on high-probability scenarios of load and RES production. Consequently, it cannot guarantee safety and reliability under extreme low-probability conditions. Future research should focus on evaluation and adjustment of capacity decisions to better accommodate these extreme low-probability scenarios of load and RES production. Additionally, an examination of the effects of detailed transmission constraints and grid expansion on the placement and sizing of renewable energy sources and energy storage systems can further refine planning approaches.

Author Contributions: Conceptualization, Z.W. and W.W.; methodology, Y.L. and W.W.; software, Y.L.; validation, S.W., S.Z. and Y.Z.; formal analysis, M.Z.; investigation, S.W.; writing—original draft preparation, W.W.; writing—review and editing, Z.W. All authors have read and agreed to the published version of the manuscript.

Funding: This research was funded by the Science and technology project of China Southern Power Grid: GDKJXM20222459.

Data Availability Statement: The original contributions presented in this study are included in the article; further inquiries can be directed to the corresponding author.

Conflicts of Interest: Authors Weijie Wu, Yixin Li, Shucan Zhou, Yining Zhang and Minjia Zheng were employed by Guangdong Power Grid Corporation, Authors Shu Wang and Zheng Wang were employed by the company China Electric Power Research Institute. Authors declare that the research was conducted in the absence of any commercial or financial relationships that could be construed as a potential conflict of interest. The authors declare that this study received funding from Southern Power Grid Company. The funder was not involved in the study design, collection, analysis, interpretation of data, the writing of this article or the decision to submit it for publication.

Appendix A

Table A1. Parameters of local areas.

	Area 1	Area 2	Area 3
$S_{n,w}^{\max}$	2200	1800	2500
$S_{n,PV}^{\max}$	1200	800	1000
$S_{n,ESS}^{\max}$	2000	1600	1000
$S_{n,s}^{w0}$	800	600	700
$S_{n,s}^{pv0}$	300	280	310
$S_{n,s}^{ESS0}$	100	120	200
$P_{n,s}^{u}$ (MW)	220	160	120
$P_{n,s}^{d}$ (MW)	−140	−120	−80

References

1. Kroposki, B.; Johnson, B.; Zhang, Y.; Gevorgian, V.; Denholm, P.; Hodge, B.-M.; Hannegan, B. Achieving a 100% renewable grid: Operating electric power systems with extremely high levels of variable renewable energy. *IEEE Power Energy Mag.* **2017**, *15*, 61–73. [CrossRef]
2. Li, Q.; Zhou, Y.; Wei, F.; Li, S.; Wang, Z.; Li, J.; Zhou, G.; Liu, J.; Yan, P.; Yu, D. Multi-time scale scheduling for virtual power plants: Integrating the flexibility of power generation and multi-user loads while considering the capacity degradation of energy storage systems. *Appl. Energy* **2024**, *362*, 122980. [CrossRef]
3. Kim, I.; Kim, W. Application of market-based control with thermal energy storage system for demand limiting and real-time pricing control. *Energy* **2023**, *263*, 125579. [CrossRef]
4. Kunya, A.B.; Abubakar, A.S.; Yusuf, S.S. Review of economic dispatch in multi-area power system: State-of-the-art and future prospective. *Electr. Power Syst. Res.* **2023**, *217*, 109089. [CrossRef]
5. Zheng, X.; Chen, H.; Xu, Y.; Liang, Z.; Chen, Y. A hierarchical method for robust scuc of multi-area power systems with novel uncertainty sets. *IEEE Trans. Power Syst.* **2019**, *35*, 1364–1375. [CrossRef]
6. Wei, Y.; Ye, Q.; Ding, Y.; Ai, B.; Tan, Q.; Song, W. Optimization model of a thermal-solar-wind power planning considering economic and social benefits. *Energy* **2021**, *222*, 119752. [CrossRef]
7. Zang, T.; Wang, S.; Wang, Z.; Li, C.; Liu, Y.; Xiao, Y.; Zhou, B. Integrated planning and operation dispatching of source–grid–load–storage in a new power system: A coupled socio–cyber–physical perspective. *Energies* **2024**, *17*, 3013. [CrossRef]
8. Zhang, B.; Huang, J. Shared energy storage capacity configuration of a distribution network system with multiple microgrids based on a stackelberg game. *Energies* **2024**, *17*, 3104. [CrossRef]
9. Li, Y.; Feng, B.; Wang, B.; Sun, S. Joint planning of distributed generations and energy storage in active distribution networks: A bi-level programming approach. *Energy* **2022**, *245*, 123226. [CrossRef]
10. Hu, J.; Wang, Y.; Dong, L. Low carbon-oriented planning of shared energy storage station for multiple integrated energy systems considering energy-carbon flow and carbon emission reduction. *Energy* **2024**, *290*, 130139. [CrossRef]
11. Xie, R.; Wei, W.; Li, M.; Dong, Z.; Mei, S. Sizing capacities of renewable generation, transmission, and energy storage for low-carbon power systems: A distributionally robust optimization approach. *Energy* **2023**, *263*, 125653. [CrossRef]
12. Artis, R.; Shivaie, M.; Weinsier, P.D. A flexibility-based multi-objective model for contingency-constrained transmission expansion planning incorporating large-scale hydrogen/compressed-air energy storage systems and wind/solar farms. *J. Energy Storage* **2023**, *70*, 108086. [CrossRef]
13. Khodaei, A.; Shahidehpour, M.; Wu, L.; Li, Z. Coordination of short-term operation constraints in multi-area expansion planning. *IEEE Trans. Power Syst.* **2012**, *27*, 2242–2250. [CrossRef]
14. Koltsaklis, N.E.; Georgiadis, M.C. A multi-period, multi-regional generation expansion planning model incorporating unit commitment constraints. *Appl. Energy* **2015**, *158*, 310–331. [CrossRef]
15. Chen, X.; Lv, J.; McElroy, M.B.; Han, X.; Nielsen, C.P.; Wen, J. Power system capacity expansion under higher penetration of renewables considering flexibility constraints and low carbon policies. *IEEE Trans. Power Syst.* **2018**, *33*, 6240–6253. [CrossRef]
16. Zhang, C.; Cheng, H.; Liu, L.; Zhang, H.; Zhang, X.; Li, G. Coordination planning of wind farm, energy storage and transmission network with high-penetration renewable energy. *Int. J. Electr. Power Energy Syst.* **2020**, *120*, 105944. [CrossRef]
17. Mehrtash, M.; Kargarian, A.; Mohammadi, A. Distributed optimisation-based collaborative security-constrained transmission expansion planning for multi-regional systems. *IET Gener. Transm. Distrib.* **2019**, *13*, 2819–2827. [CrossRef]
18. Li, Q.; Wang, J.; Chen, J.; Ding, T.; Gu, C. A hierarchical multi-area capacity planning model considering configuration ratios of renewable energy and energy storage systems with multi-area coordination. *IET Gener. Transm. Distrib.* **2023**, *17*, 3658–3677. [CrossRef]
19. Zhou, Y.; Zhai, Q.; Yuan, W.; Wu, J. Capacity expansion planning for wind power and energy storage considering hourly robust transmission constrained unit commitment. *Appl. Energy* **2021**, *302*, 117570. [CrossRef]
20. Chen, X.; Dong, W.; Yang, Q. Robust optimal capacity planning of grid-connected microgrid considering energy management under multi-dimensional uncertainties. *Appl. Energy* **2022**, *323*, 119642. [CrossRef]

21. Flores-Quiroz, A.; Strunz, K. A distributed computing framework for multi-stage stochastic planning of renewable power systems with energy storage as flexibility option. *Appl. Energy* **2021**, *291*, 116736. [CrossRef]
22. Moreira, A.; Pozo, D.; Street, A.; Sauma, E. Reliable renewable generation and transmission expansion planning: Co-optimizing system's resources for meeting renewable targets. *IEEE Trans. Power Syst.* **2016**, *32*, 3246–3257. [CrossRef]
23. Nasiri, N.; Banaei, M.R.; Zeynali, S. A hybrid robust-stochastic approach for unit commitment scheduling in integrated thermal electrical systems considering high penetration of solar power. *Sustain. Energy Technol. Assess.* **2022**, *49*, 101756. [CrossRef]
24. Baringo, L.; Baringo, A. A stochastic adaptive robust optimization approach for the generation and transmission expansion planning. *IEEE Trans. Power Syst.* **2017**, *33*, 792–802. [CrossRef]
25. Baringo, L.; Conejo, A. Correlated wind-power production and electric load scenarios for investment decisions. *Appl. Energy* **2013**, *101*, 475–482. [CrossRef]
26. Baringo, L.; Conejo, A.J. Risk-constrained multi-stage wind power investment. *IEEE Trans. Power Syst.* **2012**, *28*, 401–411. [CrossRef]
27. Mohammadi, A.; Mehrtash, M.; Kargarian, A. Diagonal quadratic approximation for decentralized collaborative tso+ dso optimal power flow. *IEEE Trans. Smart Grid* **2018**, *10*, 2358–2370. [CrossRef]
28. Kim, H.M.; Michelena, N.F.; Papalambros, P.Y.; Jiang, T. Target cascading in optimal system design. *J. Mech. Des.* **2003**, *125*, 474–480. [CrossRef]
29. Kargarian, A.; Fu, Y.; Li, Z. Distributed security-constrained unit commitment for large-scale power systems. *IEEE Trans. Power Syst.* **2014**, *30*, 1925–1936. [CrossRef]
30. Michelena, N.; Park, H.; Papalambros, P.Y. Convergence properties of analytical target cascading. *AIAA J.* **2003**, *41*, 897–905. [CrossRef]
31. Zeng, B.; Zhao, L. Solving two-stage robust optimization problems using a column-and-constraint generation method. *Oper. Res. Lett.* **2013**, *41*, 457–461. [CrossRef]
32. Yan, M.; Zhang, N.; Ai, X.; Shahidehpour, M.; Kang, C.; Wen, J. Robust two-stage regional-district scheduling of multi-carrier energy systems with a large penetration of wind power. *IEEE Trans. Sustain. Energy* **2018**, *10*, 1227–1239. [CrossRef]
33. Wang, L.; Zhang, B.; Li, Q.; Song, W.; Li, G. Robust distributed optimization for energy dispatch of multi-stakeholder multiple microgrids under uncertainty. *Appl. Energy* **2019**, *255*, 113845. [CrossRef]
34. Zhao, L.; Zeng, B. Robust unit commitment problem with demand response and wind energy. In Proceedings of the 2012 IEEE Power and Energy Society General Meeting, San Diego, CA, USA, 22–26 July 2012; IEEE: Piscataway, NJ, USA, 2012; pp. 1–8.
35. Zeng, B.; An, Y. Solving Bilevel Mixed Integer Program by Reformulations and Decomposition. Tech Rep. University of South Florida. 2014. Available online: https://api.semanticscholar.org/CorpusID:17282835 (accessed on 6 October 2024).
36. Zhang, B.; Li, Q.; Wang, L.; Feng, W. Robust optimization for energy transactions in multi-microgrids under uncertainty. *Appl. Energy* **2018**, *217*, 346–360. [CrossRef]
37. Malekpour, A.R.; Pahwa, A. Stochastic networked microgrid energy management with correlated wind generators. *IEEE Trans. Power Syst.* **2017**, *32*, 3681–3693. [CrossRef]
38. Li, Y.; Lu, Z.; Michalek, J.J. Diagonal quadratic approximation for parallelization of analytical target cascading. *J. Mech. Des.* **2008**, *130*, 051402. [CrossRef]

Disclaimer/Publisher's Note: The statements, opinions and data contained in all publications are solely those of the individual author(s) and contributor(s) and not of MDPI and/or the editor(s). MDPI and/or the editor(s) disclaim responsibility for any injury to people or property resulting from any ideas, methods, instructions or products referred to in the content.